

Volume 11
Issue 1
July 2022

ISSN - 1857 - 839X

SJCE
SCIENTIFIC
JOURNAL
OF CIVIL
ENGINEERING

SJCE
SCIENTIFIC
JOURNAL
OF CIVIL
ENGINEERING



SS CYRIL AND METHODIUS UNIVERSITY
FACULTY OF CIVIL ENGINEERING



EDITORIAL - Preface to Volume 11 Issue 1 of the Scientific Journal of Civil Engineering (SJCE)

Marijana Lazarevska EDITOR - IN - CHIEF

Dear Readers,

Scientific Journal of Civil Engineering (SJCE) is an international, peer-reviewed, open access journal published bi-annually since December 2012. As of December 2021, SJCE has its own web page and offers a completely digital submission, review, and publication process. For more information regarding the online version of the Journal, please visit www.sjce.gf.ukim.edu.mk

This Journal is committed to publish and disseminate high quality and novel scientific research work in the broad field of engineering sciences. SJCE is designed to advance technical knowledge and to foster innovative engineering solutions in the field of civil engineering, geotechnics, survey and geo-spatial engineering, environmental protection, construction management etc.

Our aim is to provide the best platform for the researchers to publish their work with transparency and integrity with the open-access model, and to provide a forum for original papers on theoretical and practical aspects of civil engineering and related sub-topics.

As an editor-in-chief of the Scientific Journal of Civil Engineering, it is my great pleasure to present you the **First Issue of Volume 11**, an open-subject issue that contains eight scientific-research papers that have passed the general review process of this journal.

These papers cover various advanced scientific topics. The first paper is dedicated to uncertainties and risks that might occur during tunnel construction, explaining the benefits of application of a risk-based approaches in tunnel engineering that contribute to better designs and safer construction. A thorough review of InSAR technology for determination of surface deformation is given in the second paper of this Issue. The third paper presents the results from the numerical analysis of non-

sway steel frame with semi-rigid connections. Despite the fact that rebonded PolyUrethane (RPU) has been used for a long time, its potential has not been extensively explored. Concerning the new strategies for sustainable and green polyurethanes, the authors of the fourth paper investigate and analyze the sound absorption properties of RPU flexible foams with different densities and thicknesses. A methodology, according to Eurocode 3, for determination of rotational stiffness of steel frames using semi-rigid connection is analyzed and presented in the fifth paper. The sixth paper explains the systematic approach of life cycle assessment as a standardized, science-based methodology that has been developed to evaluate the environmental impact of buildings, with respect to their processes, their materials and use (energy) throughout the whole life cycle. An overview of the actual state of the railway infrastructure in Republic of North Macedonia is given in the seventh paper, considering the track deterioration from geometric aspects and its influencing factors. Embracing the principles of sustainability, the authors of the final paper present an interesting approach for preserving an outdated and abandoned industrial buildings.

I sincerely hope that all papers published in this issue will encourage further researches on the fields.

I thank all the authors for contributing to this Issue and all the reviewers for providing detailed and timely evaluations of the submitted manuscripts. Furthermore, I would like to express my sincere gratitude to all editor members for their excellent work, remarkable contribution, enthusiasm and support.

Sincerely Yours, Assoc. Prof. Dr. Marijana
Lazarevska
July, 2022

Impressum

FOUNDER AND PUBLISHER

Faculty of Civil Engineering
Partizanski odredi 24, 1000
Skopje, N. Macedonia

PRINT

This Journal is printed in Mar-saz
DOOEL Skopje

EDITORIAL OFFICE

Faculty of Civil Engineering
Partizanski odredi 24, 1000
Skopje, N. Macedonia
tel. +389 2 3116 066
fax. +389 2 3118 834
prodekan.nauka@gf.ukim.edu.mk

EDITOR IN CHIEF

Assoc. Prof. PhD **Marijana Lazarevska**
University "Ss. Cyril and Methodius"
Faculty of Civil Engineering
Partizanski odredi 24, 1000
Skopje, N. Macedonia
marijana@gf.ukim.edu.mk

EDITORIAL ADVISORY BOARD

Prof. PhD **Elena Dumova-Jovanoska**
University "Ss. Cyril and Methodius", Skopje, N. Macedonia

Assoc. Prof. PhD **Zlatko Bogdanovski**
University "Ss. Cyril and Methodius", Skopje, N. Macedonia

TECHNICAL EDITORS

MSc **Milica Jovanoska**
Assistant, University "Ss. Cyril and Methodius", Skopje, N. Macedonia

PhD **Kristina Milkova**
Assistant, University "Ss. Cyril and Methodius", Skopje, N. Macedonia

MSc **Riste Volcev**
Assistant, University "Ss. Cyril and Methodius", Skopje, N. Macedonia

ISSN: 1857-839X

EDITORIAL BOARD

Rita Bento, PhD
Instituto Superior Técnico,
Universidade de Lisboa,
Department of Civil Engineering,
Architecture and Georesources,
Lisbon, Portugal

Zlatko Bogdanovski, PhD
University "Ss. Cyril and Methodius", Faculty of Civil Engineering, Skopje, N. Macedonia

Heinz Brandl, PhD
Vienna University of Technology,
Institute for Geotechnics, Vienna,
Austria

Maosen Cao, PhD
Hohai University, Department of Engineering Mechanics, Nanjing, China

Eleni Chatzi, PhD
ETH Zurich, Chair of Structural Mechanics & Monitoring, Zurich, Switzerland

Tina Dasic, PhD
University of Belgrade, Faculty of Civil Engineering, Belgrade, R. Serbia

Ljupco Dimitrievski, PhD
University "Ss. Cyril and Methodius", Faculty of Civil Engineering, Skopje, N. Macedonia

Katerina Donevska, PhD
University "Ss. Cyril and Methodius", Faculty of Civil Engineering, Skopje, N. Macedonia

Elena Dumova-Jovanoska, PhD
University "Ss. Cyril and Methodius", Faculty of Civil

Engineering, Skopje, N. Macedonia

Michael Havbro Faber, PhD
Aalborg University, Department of Civil Engineering, Aalborg, Denmark

Massimo Fragiaco, PhD
University of L'Aquila, Department of Civil, Construction-Architectural & Environmental Engineering, L'Aquila, Italy

Tomas Hanak, PhD
Brno University of Technology, Faculty of Civil Engineering, Brno, Czech Republic

Nenad Ivanisevic, PhD
University of Belgrade, Faculty of Civil Engineering, Belgrade, R. Serbia

Milos Knezevic, PhD
University of Montenegro, Faculty of Civil Engineering, Podgorica, Montenegro

Andrej Kryzanowski, PhD
University of Ljubljana, Faculty of Civil and Geodetic Engineering, Ljubljana, Slovenia

Stjepan Lakusic, PhD
University of Zagreb, Faculty of Civil Engineering, Zagreb, Croatia

Marijana Lazarevska, PhD
University "Ss. Cyril and Methodius", Faculty of Civil Engineering, Skopje, N. Macedonia

Peter Mark, PhD
Ruhr University, Faculty of Civil and Environmental Engineering, Bochum, Germany

Marc Morell
Institute des Sciences de l'Ingénieur de Montpellier, France

Impressum

Vlastimir Radonjanin, PhD

University of Novi Sad, Faculty of
Technical Sciences, Novi Sad , R.
Serbia

Marina Rakocevic, PhD

University of Montenegro, Faculty
of Civil Engineering, Podgorica,
Montenegro

Resat Ulusay, PhD

Hacettepe University, Faculty of
Engineering, Ankara, Turkey

Joost C. Walraven, PhD

Delft University of Technology,
Department of Civil Engineering,
Delft, Netherlands

Zlatko Zafirovski, PhD

University "Ss. Cyril and
Methodius", Faculty of Civil
Engineering, Skopje, N.
Macedonia

Ales Znidaric, PhD

ZAG – Slovenian National Building
and Civil Engineering Institute,
Ljubljana, Slovenia

COVER DESIGN:

Prof. PhD **Mitko Hadzi Pulja**
Mr. Arh **Darko Draganovski**
Faculty of Architecture
University "Ss. Cyril and
Methodius", Skopje, N. Macedonia

ORDERING INFO

SJCE is published bi-annually.
All articles published in the journal
have been reviewed.
Edition: 100 copies

SUBSCRIPTIONS

Price of a single copy:
for Macedonia (500 den);
for abroad (10 EUR + shipping
cost).

**BANKING DETAILS
(NORTH MACEDONIA)**

Narodna banka na RNM
Account number:
160010421978815
Prihodno konto 723219,
Programa 41

**BANKING DETAILS
(INTERNATIONAL)**

Correspond bank details:
Deutsche Bundesbank Zentrale
Address: Wilhelm Epstein Strasse
14 Frankfurt am Main, Germany
SWIFT BIC: MARK DE FF
Bank details:
National Bank of the RNM
Address: Kompleks banki bb 1000
Skopje North Macedonia
SWIFT BIC:NBRM MK 2X
IBAN: MK 07 1007 0100 0036 254
Name: Gradezen fakultet Skopje



WWW.GF.UKIM.EDU.MK



WWW.GF.UKIM.EDU.MK

V. Gacevski, V. Zileska Pancovska, M. Lazarevska ASSESSMENT OF RISKS IN A ROAD TUNNEL CONSTRUCTION USING TREE ANALYSIS	7
T. Gegovski, Z. Bogdanovski, F. Kasapovski A REVIEW OF INSAR TECHNOLOGY FOR DETERMINATION OF SURFACE DEFORMATION	13
D. Memedi, D. Popovski, M. Partikov, A. Nasufi ANALYTICAL MODEL OF NON-SWAY STEEL FRAME WITH SEMI-RIGID CONNECTIONS	21
V. Mickovski, G. Iannace, M. Jovanoska-Mitrevska, T. Samardzioska REBONDED POLYURETHANE FLEXIBLE FOAM AS SOUND ABSORBING MATERIAL	27
A. Nasufi, D. Popovski, M. Partikov, D. Memedi OPTIMIZATION OF STEEL FRAMES USING SEMI-RIGID CONNECTIONS	35
M. Naumovski, M. Lazarevska, D. Dimkovski COMFORT, AS AN ASPECT OF LIFE CYCLE ASSESSMENT (LCA) ANALYSIS TOWARD SUSTAINABLE BUILDINGS	41
I. Nedevska, Z. Zafirovski, M. Lazarevska, R. Ristov, V. Gacevski TRACK GEOMETRY DEGRADATION AND MAINTENANCE OF THE RAILWAYS	55
H. Pasternak, N. Živaljević-Luxor THE COLOSSUS OF PRORA – BUILDING HISTORY AND NEW BEGINNING	61

HOW WOULD YOU TAKE YOUR STUDYING?

STAY IN



TAKEOUT



ON THE GO



Vasko Gacevski

MSc, Teaching Assistant
University “Ss. Cyril and Methodius”
Faculty of Civil Engineering – Skopje
gacevski@gf.ukim.edu.mk

Valentina Zileska Pancovska

PhD, Full Professor
University “Ss. Cyril and Methodius”
Faculty of Civil Engineering – Skopje
valentinazp@gf.ukim.edu.mk

Marijana Lazarevska

PhD, Assistant Professor
University “Ss. Cyril and Methodius”
Faculty of Civil Engineering – Skopje
marijana@gf.ukim.edu.mk

ASSESSMENT OF RISKS IN A ROAD TUNNEL CONSTRUCTION USING TREE ANALYSIS

Nowadays, new technologies, materials and machines enable the application of tunnel solutions even in the most difficult construction conditions. However, even with the great progress in tunneling, uncertainties and risks are always present in this field. In this direction, risks in tunnel construction should be appropriately analyzed and managed. This paper shows a methodology for risk assessment of road tunnels using combination of fault and event tree analysis. The fault tree is used for determination of the probabilities of previously estimated hazards and the event tree defines the consequences and the risks during a road tunnel construction in a quantitative form. The use of such approach can contribute to more successful tunneling project.

Keywords: tunnels, construction uncertainties and hazards, risk assessment, tree analysis

1. INTRODUCTION

Tunneling is a specific area of civil engineering that is associated with dangers during project execution. Dangers impose hazards on all parties involved not only on those directly engaged with the task [1]. Therefore worldwide exists an increasing trend for the application of risk-based approaches to increase awareness of this issue. In that sense risk assessment is a structured process that identifies the probability and degree of negative consequences resulting from certain natural events or human activities (hazard) [2].

In R. N. Macedonia according to the current and future project solutions for the road and railway corridors, the construction of a significant number of tunnels is in sight. These tunnels have different characteristics and conditions, which means that various risks can occur during construction [3]. Neglecting the risk during construction can lead to increased costs and delays in the project [4]. In some cases, negative impact to the environment and people can occur. Thus, risk analysis and management is becoming mandatory part of tunnel engineering, contributing to better design and safer construction.

2. RISKS IN TUNNELING

Generally, risks in tunneling construction can be associated with economic losses and less often with human, environmental and other consequences. The data from the most significant tunnel losses in the past few decades shows that the most frequent causes are [5]:

- Insufficient ground investigation and/or interpretation;
- Faulty design and/or workmanship (construction);
- Lack of appropriate measures or procedures on site which would enable the timely recognition of imminent problems.

This shows that tunnel risks should be assessed and managed in every project phase [6]. For a long time tunnel accidents during construction have been connected with a significant number of human victims. A drastic reduction in fatal injuries comes with the emergence and application of newer tunneling methods and technologies [7,8]. But even nowadays there are still human fatalities and injuries. In May 2022 during the construction of the Khooni Nallah tunnel in India, 10 workers died after a collapse [9].

1.1 TYPES OF RISK ASSESSMENT

There are different types of risk assessment that can be used in various project phases. The first and simpler one is the qualitative risk assessment. This type is mostly used in earlier project stages while major changes in the design part are still possible [10]. Usually this is done in a form of a risk register [4].

In later project phases, when more information and data is available, the quantitative approach is adequate for risk assessment. This type of assessment can be used during the making of the final (main) design, before or after construction start. The quantification of uncertainties, hazards and risks represents a combination of graphical and mathematical approaches or models such as analysis, artificial networks, studies and processes. Some of the used quantitative approaches are: fault, event and decision tree analysis, neural and Bayesian networks, failure mode and effects analysis, multicriteria decision analysis, Markov Analysis, etc [2, 11, 12].

2.1.1 Fault tree analysis

This approach serves to analyze a particular hazard and different ways and reasons that cause it. The fault tree itself is a graphical model that shows a combination of observable events or uncertainties (preceding the potential hazard). The nature of the particular graphical model is qualitative, but due to its particular suitability for quantification, it is often used in combination with probabilistic models (figure 1). From the top (main) event, the tree is logically branched to the basic events that contribute to the probability of failure or occurrence of the top event [5, 13].

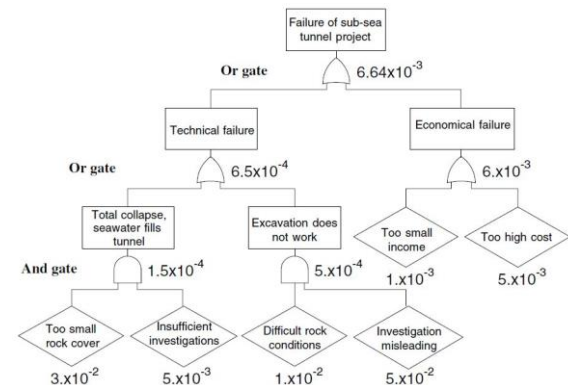


Figure 1. Example of a fault tree for a failure of a sub-sea tunnel project [10]

2.1.2 Event tree analysis

The description of the development from an initial event through possible sequences to a defined final state can be carried out through event tree analysis. This technique identifies and analyses possible scenarios that follow a certain initial event (hazard). The tree of events allows, through a logical and overview order, to determine the consequences that may occur in the project (figure 2) [14].

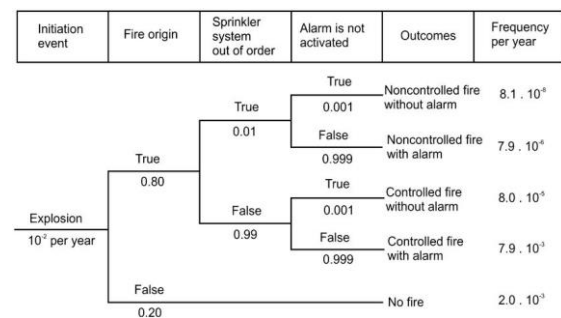


Figure 2. Example of an event tree analysis for an explosion in tunnel [15]

3. ROAD TUNNEL RISK ASSESSMENT

With a combination of the fault and event tree, we can assess previously defined hazards and the consequences they cause regarding the success or failure of some construction measures. After the definition of the structure of the trees, probabilities are assigned for each event, after which the probability of the top event (hazard) is calculated. This top event with its probability represents the initiating event in the event tree. The event tree is then branched using three main measures that mostly affect the outcome. In this paper, this type of combination is shown for a road tunnel.

The tunnel is part of the future highway line in the west part of North Macedonia (Gostivar-Kicevo) on the European transport corridor VIII. It's a standard highway tunnel solution with two tunnel pipes ($L_1=622,0m$; $L_2=705,8m$). The risk assessment is done for the construction phase (which is not started) using all the data and information from the design phase. The available data consist of studies, reports and project documentation (main design) regarding tunnel position, geometry and support, geology, ground investigations and classification.

With previously conducted qualitative risk assessment, three hazards were chosen for the quantitative approach. The results from the fault tree are shown in table 1 for each hazard different fault and event trees were constructed with different probabilities for the basic events. Additionally for the highest probability hazard, using the lognormal distribution and advanced Monte Carlo simulation with 1000 samples, results were obtained in the form of a cumulative probability distribution.

Table 1. Results from the fault tree analysis

Hazard	Probability of occurrence
Unpredicted groundwater inflow (flooding)	0,0420 (4,20 %)
Instability of the excavation face (face collapse)	0,0874 (8,74 %)
Instability of rock blocks (rock fall)	0,1626 (16,26 %)

By applying these hazard occurrence probabilities and assigning failure probabilities to preventive measures (risk reduction measures) in the event tree, the risk results were obtained (table 2). For each hazard there are three types of preventive measures:

grouting (forepoling), primary support (timely adequate installation) and cavity filling (concrete or cement). Their success or failure represented by a probability, determines the risk outcome.

Table 2. Results from the event tree analysis

Risk	Probability of occurrence
Unpredicted groundwater inflow (flooding)	0,0000210 (0,00210 %)
Instability of the excavation face (face collapse)	0,0000874 (0,00874 %)
Instability of rock blocks (rock fall)	0,0001626 (0,01626 %)

For the instability of rock blocks, the additional probabilistic analysis was conducted. The results are shown in table 3 and 4.

Table 3. Results from the probabilistic fault tree analysis

Primary value	0,1626
Mean value	0,1624
Standard deviation	0,0509
5 %	0,0962
50 %	0,1518
95 %	0,2571

Table 4. Results from the probabilistic event tree analysis

Primary value	0,0001626
Mean value	0,0001573
Standard deviation	0,0001516
5 %	0,0000256
50 %	0,0001081
95 %	0,0007240

Figure 3 shows the fault tree for the instability of rock blocks (rock fall) with the logical branching and the probabilities of all the events. There are three main groups below the top event: previous data, construction technology, instruments and monitoring. Figure 4 shows the event for the instability of rock blocks with the preventive measures and the probabilities of all the events. The top branching represent the worst scenario where all the measures fail and we have severe consequences.

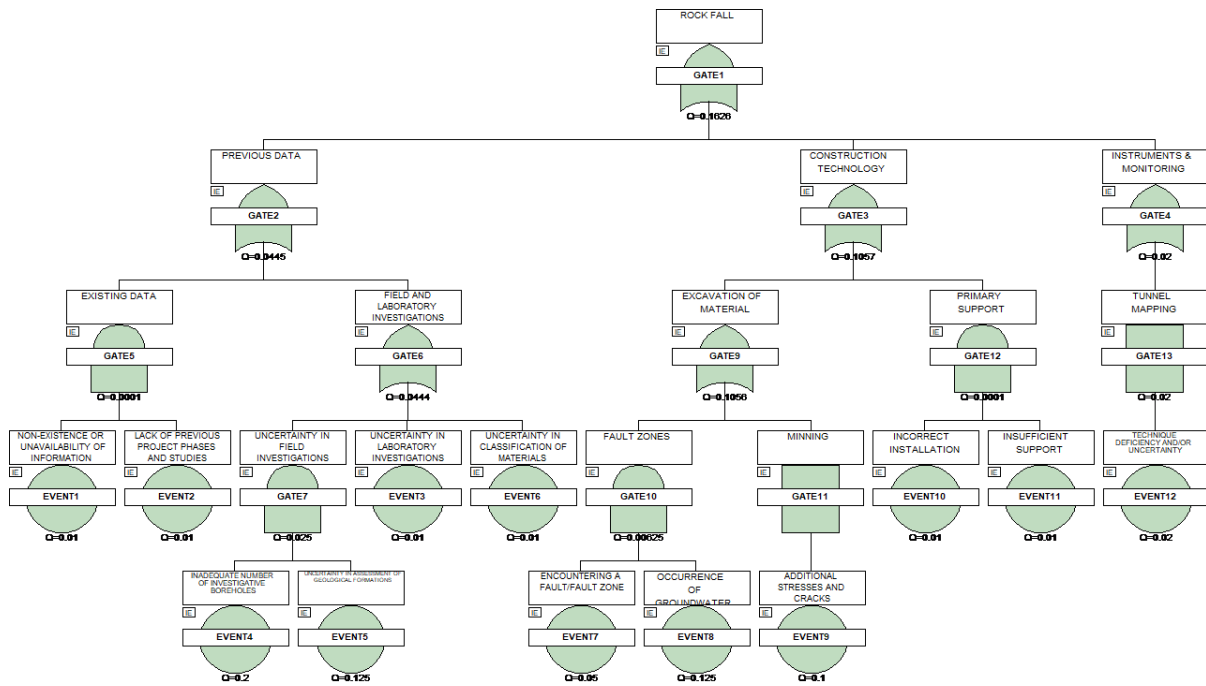


Figure 3. Fault tree for instability of rock blocks (rock fall)

Hazard initial (top) event	GROUTING	PRIMARY SUPPORT	CAVITY FILLING	Consequence	Result
----------------------------	----------	-----------------	----------------	-------------	--------

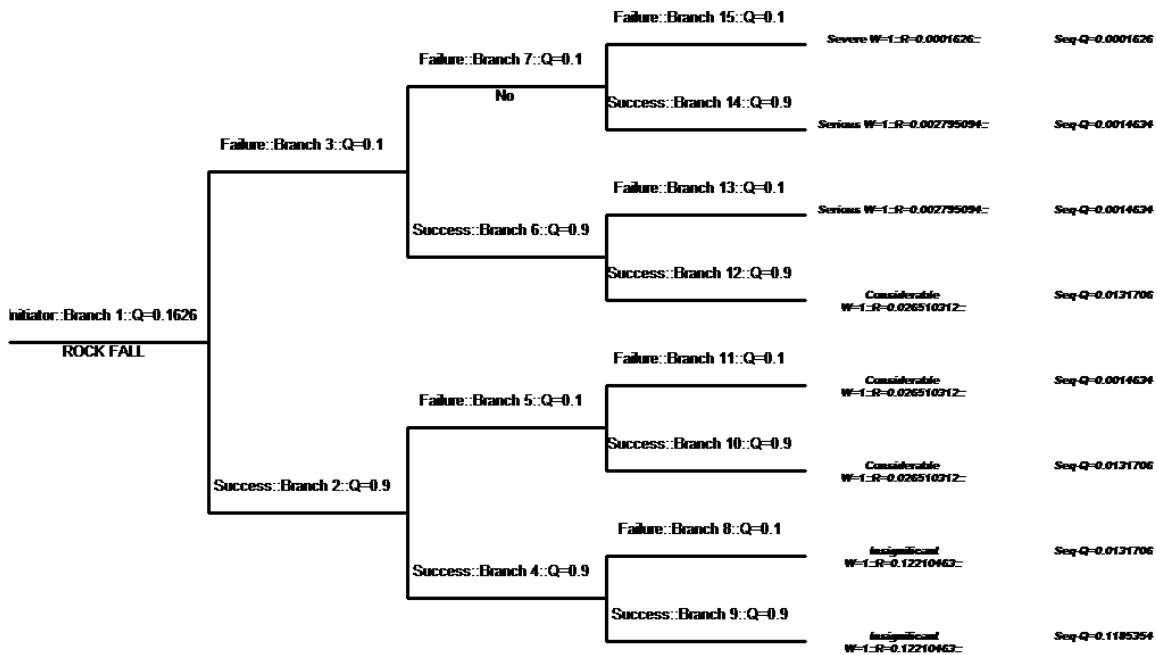


Figure4. Event tree for instability of rock blocks (rock fall)

4. CONCLUSIONS

Risks are always present in tunnel engineering. From planning, through design and finally in the construction phase risks can have a major influence for the project. Neglecting this

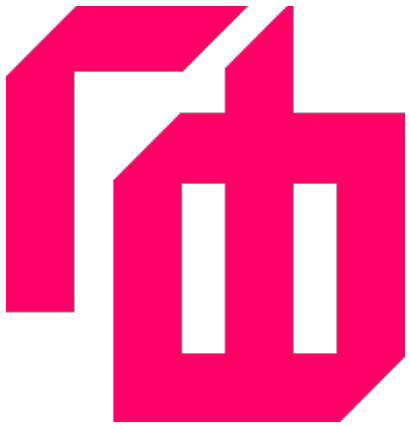
problem can only lead to unpredicted consequences that usually have negative impact. This paper shows a combination of tree analysis models that can be used for quantitative risk assessment. First with the fault tree, the hazards can be analyzed, resulting in probability of occurrence or failure for each

event. Afterwards in the event tree we can analyze different scenarios and consequences that follow every hazard. The shown assessment refers to a road tunnel, where the data from the design phase is used for the determination of risks that can occur during construction. Three main hazards are analyzed with to combination of the fault and event tree. Additionally for the highest risk, a cumulative probability distribution was implemented. The fault tree for this risk shows that the construction technology has the biggest influence in the hazard occurrence. The event tree presents the effectiveness of the

preventive (remedial) measures and in the end the consequences i.e. the risks from each scenario. The determination and classification of the assessed risks should be made in the management phase. This next step should define the acceptable levels of risk and different actions to be carried out based on the classification. This kind of approach to risk throughout assessment and management can benefit all the project participants and cause safe and reliable working environment.

REFERENCES

- [1] Morris M. S., Gopalakrishna V. D. (2020). „Development of a Risk Management Framework for Tunnel Construction in India“, International Journal of Engineering Research & Technology (IJERT), Vol. 9 Issue 06, June-2020.
- [2] Pamukcu C. (2015). „Analysis and management of risks experienced in tunnel construction“, Acta Montanistica Slovaca, Volume 20, number 4, pp. 271-281.
- [3] Seidenfus T. (2006). „Collapses in Tunnelling“, Stuttgart University of Applied Sciences, MSc Thesis.
- [4] Zafirovski Z., Gacevski V., Lazarevska M., Ognjenovic S. (2019) „Procedures for risk analysis and management in tunnelling projects“, E3S Web of Conferences 135, 01001.
- [5] Sousa L. R. (2010). „Risk Analysis for Tunneling Projects“, Massachusetts Institute of Technology, Department of Civil and Environmental Engineering, PhD Thesis.
- [6] Ghasemi Y., Ardeshir A., Amiri M. (2012). „Risk Identification and Fault Tree Development of Urban Tunnel Projects“ in Advancing Civil, Architectural and Construction Engineering & Management, proceedings of the Third International Conference on Construction in Developing Countries (ICCIDC-III), July 2012, Bangkok, Thailand.
- [7] Kikkawa N., Itoh K., Hori T., Toyosawa Y., Orense P. R. (2015). „Analysis of labour accidents in tunnel construction and introduction of prevention measures“, Industrial Health, Volume 53, pp. 517-521.
- [8] Tender L. M., Martins F. F., Couto P. J., Perez C. A. (2017). „Study on prevention implementation in tunnels construction: Marão Tunnel's (Portugal) singularities“, Revista de la Construcción. Journal of Construction, Vol.16 No.2, pp. 262-273.
- [9] KL News Network (2022, May, 21). *Khooni Nallah Tunnel Collapse: Ten Bodies Recovered, Negligence Case Registered*. <https://kashmirilife.net/khooni-nallah-tunnel-collapse-ten-bodies-recovered-negligence-case-registered-292899/>
- [10] Eskesen D. S., Tengborg P., Kampmann J., Veicherts H. T. (2004), „Guidelines for tunnelling risk management: International Tunnelling Association“, Working Group No. 2.
- [11] Yang R., Deng Y. (2021). „Analysis on Security Risks in Tunnel Construction Based on the Fault Tree Analysis“, IOP Conf. Series: Earth and Environmental Science 638, 012089.
- [12] Yoe C. (2019), Principles of Risk Analysis – Decision Making Under Uncertainty, Second Edition, CRC Press.
- [13] Hyun C. K., Min S., Choi H., Park J., Lee M. I. (2015). „Risk analysis using fault-tree analysis (FTA) and analytic hierarchy process (AHP) applicable to shield TBM tunnels“, Tunnelling and Underground Space Technology 49, pp. 121-129. Kikkawa N., Itoh K., Hori T., Toyosawa Y., Orense P. R. (2015). „Analysis of labour accidents in tunnel construction and introduction of prevention measures“, Industrial Health, Volume 53, pp. 517-521.
- [14] Shpackova O. (2012) „Risk management of tunnel construction projects“ Doctoral Thesis, Faculty of Civil Engineering, Czech Technical University in Prague.
- [15] Senovsky M., Senovsky P. (2008). „Critical Infrastructure Risks“. Communications - Scientific Letters of the University of Zilina 1/2008, pp. 54-59.



СЕКОГАШ
БИДИ



Tome Gegovski

MSc, assistant

Ss. Cyril and Methodius University
Faculty of Civil Engineering – Skopje
email: gegovski@gf.ukim.edu.mk

Zlatko Bogdanovski

PhD, Associate professor

Ss. Cyril and Methodius University
Faculty of Civil Engineering – Skopje
email: bogdanovski@gf.ukim.edu.mk

Filip Kasapovski

PhD, assistant

Ss. Cyril and Methodius University
Faculty of Civil Engineering – Skopje
email: kasapovski@gf.ukim.edu.mk

A REVIEW OF INSAR TECHNOLOGY FOR DETERMINATION OF SURFACE DEFORMATION

InSAR (Synthetic Aperture Radar Interferometry) is a modern technology in the field of remote sensing that allows determination of deformations of the Earth's crust for large areas with relatively high accuracy.

In this work are presented basic characteristics of InSAR technology and advance InSAR techniques: Differential InSAR (DInSAR) and Permanent Scatterer (PSInSAR).

Keywords: SAR Interferometry, DInSAR, PSInSAR, vertical deformation, geodynamics

1. INTRODUCTION

The Earth's surface is constantly under the influence of seismic processes that cause deformations. The determination of this phenomenon is in the domain of geodetic science, in the field of geodynamics.

The use of classical geodetic methods give excellent results in terms of accuracy. But these methods cannot be used for monitoring deformations on large areas.

The development of satellite technology has great significance for geodetic science because it enables measurements over great distances. The result of this is the development of satellite geodesy and remote sensing.

In the field of remote sensing, the invention of SAR sensors is particularly important, which enable the broadcast of numerous radar signals that are covering large areas of the Earth. These satellite images are the basis for SAR interferometry which allows the determination of deformations, while this technology primarily refers to the obtain of vertical displacement. In the last two decades, several methodologies have been developed for the processing of SAR images, including: DInSAR and PSInSAR, which provide accuracy of few millimeters in determining vertical deformations.

2. BASICS OF SYNTHETIC APERTURE RADAR (SAR)

SAR sensors are designed to permanently emit and receive radar signals, which register the amplitude and phase of the surface's reflected signals. These sensors are used as an integral part of specially launched satellites that orbit at a distance of about 500 to 800 km. Satellites moving around the Earth constantly broadcast a large number of signals, day and night, 365 days a year. Part of the reflected signals are returned to the SAR sensor of the satellite, and a registered in the form of a SAR image with data containing the amplitude and phase of the signal in each pixel of the SAR image. The angle (θ) between true north-south and the satellite orbit varies slightly, depending on the satellite. Generally, is in the range of 20 to 50 degrees, depending of the satellite. (Fig. 1) [14]

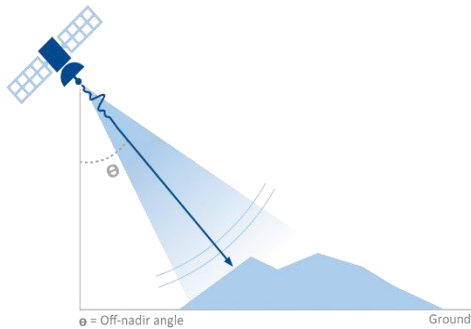


Fig.1 SAR image acquisition (<https://site.tre-altamira.com/insar/>)

Depending on the structural elements of the SAR sensor, several types of signals are used that have a characteristic frequency and wavelength. (Fig. 2) The most commonly used signals for InSAR purposes are: X-band, C-band and L-band. [5]

The SAR image is a matrix of pixels, where each pixel contain data on the amplitude and phase of the reflected signal from the Earth's

Band	Frequency	Wavelength	Typical Application
Ka	27–40 GHz	1.1–0.8 cm	Rarely used for SAR (airport surveillance)
K	18–27 GHz	1.7–1.1 cm	rarely used (H ₂ O absorption)
Ku	12–18 GHz	2.4–1.7 cm	rarely used for SAR (satellite altimetry)
X	8–12 GHz	3.8–2.4 cm	High resolution SAR (urban monitoring,; ice and snow, little penetration into vegetation cover; fast coherence decay in vegetated areas)
C	4–8 GHz	7.5–3.8 cm	SAR Workhorse (global mapping; change detection; monitoring of areas with low to moderate penetration; higher coherence); ice, ocean maritime navigation
S	2–4 GHz	15–7.5 cm	Little but increasing use for SAR-based Earth observation; agriculture monitoring (NISAR will carry an S-band channel; expands C-band applications to higher vegetation density)
L	1–2 GHz	30–15 cm	Medium resolution SAR (geophysical monitoring; biomass and vegetation mapping; high penetration, InSAR)
P	0.3–1 GHz	100–30 cm	Biomass. First p-band spaceborne SAR will be launched ~2020; vegetation mapping and assessment. Experimental SAR.

Fig.2 SAR signals (<https://www.earthdata.nasa.gov/learn/backgrounders/what-is-sar>)

surface. The amplitude is related to the energy of the backscattered signal. It means solid objects (natural or artificial) have a strong reflexivity and the amplitude of the reflected signal is high. The phrase is used in estimating displacement in interferometric application.

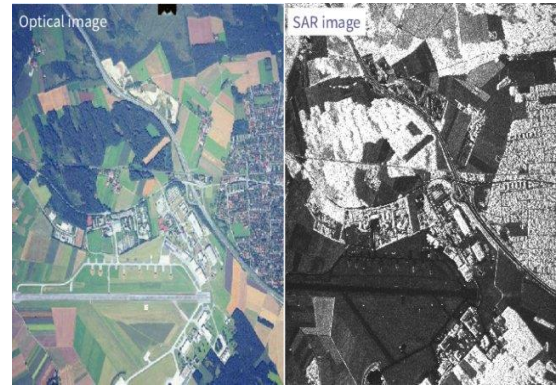


Fig.3 Optical image vs SAR image [2]

The reference frame of a SAR image is defined by the SAR coordinates: range and azimuth. (Fig. 4) Since the radar is not orthogonal to the ground, terrain elevation will result in geometric distortions in the SAR image. In fact, even the variation in the projection of the reference surface (ellipsoid) in range direction, causes geometric distortions, due to the varying incidence angle. [9]

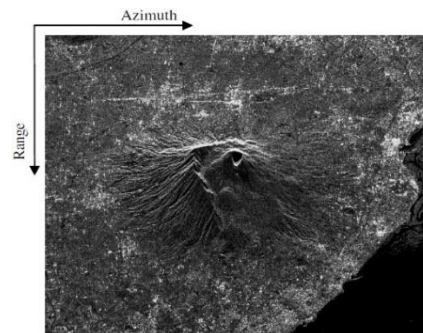


Fig.4 SAR coordinates (<https://site.tre-altamira.com/insar/>)

3. BASICS OF SAR INTERFEROMETRY

InSAR (SAR Interferometry) is a process of determining the phase differences for each pixel from a pair of SAR images acquired at different time periods, on the same surface of the Earth from the same satellite in the identical orbit.

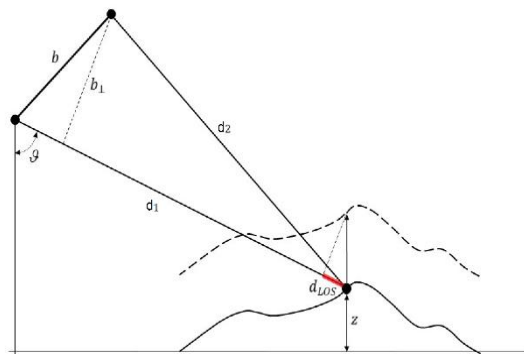


Fig.5 Sketch of the geometry interferometric SAR acquisition (<https://www.mdpi.com/2072-4292/13/23/4756>)

For every SAR pixel of the scene, the mathematical expressions for the returning of complex value signal related to the two SAR images are:

$$i_1 = \gamma_1 \exp \left[-j \frac{4\pi}{\lambda} d_1 \right]$$

$$i_2 = \gamma_2 \exp \left[-j \frac{4\pi}{\lambda} d_2 \right]$$

Where, γ_1 и γ_2 are reflective function values, d_1 и d_2 are distances from the SAR sensor to the object in both acquisitions, λ is the wavelength. The phase difference ($\Delta\phi$) can be expressed by the following mathematical expression: [1]

$$\Delta\phi = \frac{4\pi}{\lambda} \frac{b_{\perp}}{r_1 \sin \vartheta} z + \frac{4\pi}{\lambda} d_{LOS} + \Delta\phi_{atm.} + n$$

Where, z is altitude, d_{LOS} projection of the 3D deformation vector of the line of side (LOS) between two acquisitions, b_{\perp} is perpendicular baseline, ϑ is the angle of inclination of the SAR sensor and $\Delta\phi_{atm.}$ is the phase shift predicted depending the different atmospheric conditions during the acquisition period of the two SAR images.

A very important prerequisite is that the acquisition of the pair of SAR images should be registered from a similar position (ideally, the satellite would be at an identical position in the orbit during both acquisitions).

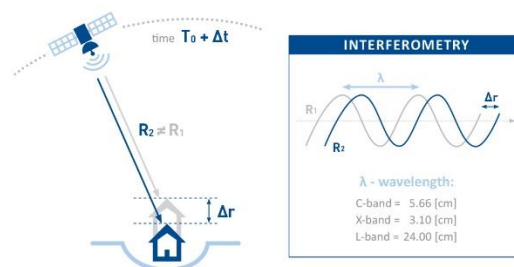


Fig.6 SAR Interferometry (<https://site.tre-altamira.com/company/>)

The result of InSAR processing is the interferogram, which is matrix of pixels with known differential interferometric phase ($\Delta\phi$) given in values from $-\pi$ to $+\pi$, express through the so-called color fringes. One fringe is equal on one cycle of the spectrum colors from purple to red, which equals the displacement that corresponds to half of the wavelength. If the color sequence is from purple to red, then ground moved away from the satellite and its show that we have ground subsidence. If the color sequence is from red to purple, then ground has moved towards the satellite and it shows that we have ground uplift. [15]

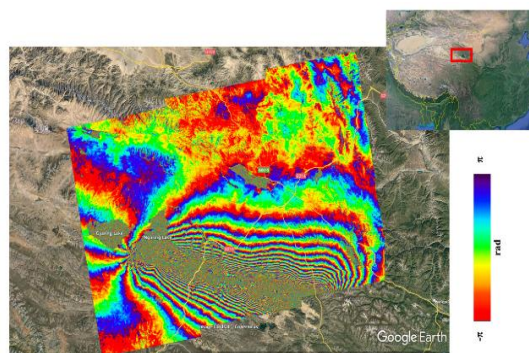


Fig.7 SAR Interferogram (<https://www.mdpi.com/2072-4292/13/23/4756/html>)

Interferometric fringes can only be observed where scene has a big coherence. The coherence in InSAR means when area on the ground appears to have surface characterization in all SAR images analyzed in all pixels. The coherence is expressed for all pixels separately in range of 0 to 1, 0 means no coherence in pixel and 1 means absolute coherence. In general, for successful determination of displacements the average coherence should be higher than 0.5. [13]

If the coherence satisfies the suggested values, the total displacement can be expressed:

total displacement (d_{LOS}) =
 number of fringers \times half wavelength

However, the acquisition of SAR images is done on the surface of the Earth in different weather conditions. It causes phase difference in the interferogram which is not equal to the intensity of the displacement, but is a combination of several additional factors, represented in the following mathematical expression:

$$\Delta\varphi = \Delta\varphi_{disp.} + \Delta\varphi_{flat} + \Delta\varphi_{elev.} + \Delta\varphi_{atm.} + \Delta\varphi_n.$$

where, $\Delta\varphi_{flat}$ is Earth's flat phase due to Earth's curvature, $\Delta\varphi_{elev.}$ is topographic correction, $\Delta\varphi_{atm.}$ is atmospheric correction such as: different humidity, temperature, pressure between two acquisitions and $\Delta\varphi_n.$ is noise which causes temporal change of scatterers, different capture angles etc. [15]

The need to remove these phase disturbances is the need for the appearance of several InSAR techniques, among which are DinSAR and PSInSAR.

3.1. DINSAR

The process of interferometric analysis of the displacements of single pair SAR images excluded from the influences of the Earth's curvature and terrain topography is called DInSAR. This technique uses a Digital Elevation Model (DTM) of the area of interest. The word "differential" refers to the removal of the topographic phase correction from the interferogram.

After implementation of the DTM, the above expression is transformed with the removal of the influence of $\Delta\varphi_{flat}$ and $\Delta\varphi_{elev.}$ and has the following form: [13]

$$\Delta\varphi_{interf.} = \Delta\varphi_{disp.} + \Delta\varphi_{atm.} + \Delta\varphi_{noise} + \varepsilon$$

where ε is the sum of possible errors in the DTM.

These processings are done exclusively using software algorithms, that do an individual calculation for each pixel in a single pair of SAR images.

The scheme of DInSAR processing in the SNAP software (Sentinel-1 Toolbox) developed by European Space Agency (ESA), with using the SLC data from Sentinel - 1 satellite is given in Fig.8 [10]

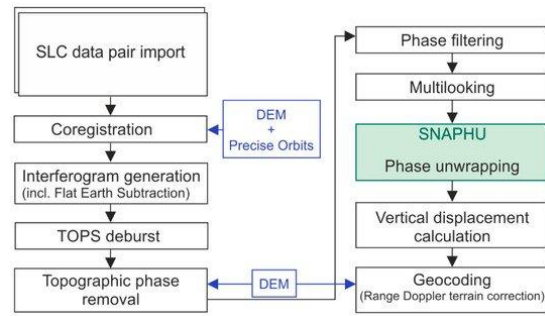


Fig.8 DInSAR scheme processing [7]

However, the vertical deformations determined by the DInSAR technique are filled with errors from atmospheric influences which can significantly affect the accuracy. This technique is usually used to review vertical displacements of significant intensity and serves as a basis for using some of the advanced techniques (such as PSInSAR), which use time series to remove atmospheric influences and obtain vertical deformations with millimeter accuracy.

3.2. PSINSAR

PSInSAR (Persistent Scatterer Interferometry) is advance technique for surface displacement determination. The first PSInSAR algorithm appeared in 1999, in the PS Technique by Politecnico di Milano (Polimi). [3]

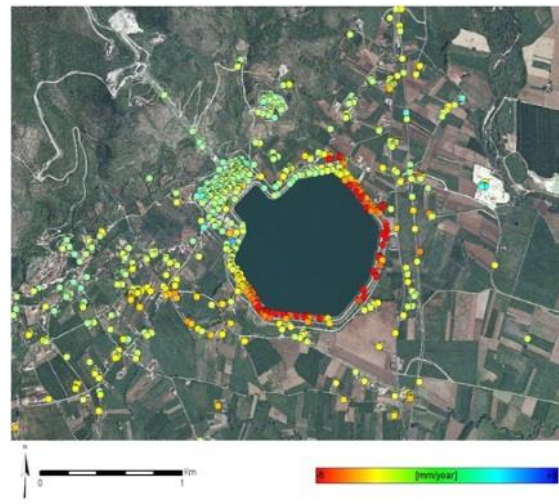


Fig.9 Permanent Scatterer (PS) and Distributed Scatterer (DS) [3]

PSI technologies are advanced forms of DInSAR, where the fundamental difference is that PSI technologies develop multiple interferograms from a stack of radar images. As a minimum of 15 SAR image are usually required for PSI algorithm. In fact, PSI represent a specific class of DInSAR with appropriate data processing and analysis procedures to separate $\Delta\varphi_{disp.}$ of the other

components represented in final equation of the DInSAR.

A Permanent Scatterer (PS) is defined as a radar target, within a resolution cell, that displays stable amplitude properties and coherent signal phase, throughout all of the images within a data stack. Objects that make good PS are varied and can be natural or artificial. Natural PS forms usually are: rock outcrops, un-vegetated earth surface, boulders etc., among the artificial object: buildings, street lights, bridge parapets, above-ground pipelines, appurtenances on dams and roof structures, and any rectilinear structure that can create a dihedral signal reflection back to the satellite. [13]

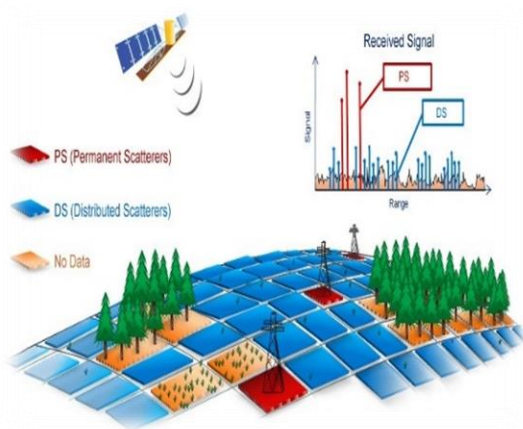


Fig.10 Permanent Scatterer (PS) and Distribute Scatterer (DS) [3]

In the paper “Analysis of Permanent Scatterers in SAR interferometry” the authors presented statistical analysis of the PS density in urban areas as a function of the standard deviation of the phase differences where in urban areas

about 100 PS/km² can be identified and exploited for terrain deformation monitoring with millimetric accuracy. [8]

The last evolution of PSInSAR technology is SqueeSAR developed by Tele - Rilevamento Europa in collaboration with Politecnico di Milano. SqueeSAR technique searches for targets in the radar image set that consistently reflect radar signals throughout the entire dataset of images, exploiting both permanently scattering ground targets: PS like buildings, pipelines, linear structures, open outcrops etc. and homogenous distributed scatterers (DS), for e.g., homogeneous ground or scattered outcrops, uncultivated areas, debris covered areas. (Fig. 10) [3]

These two InSAR techniques are very important and used for the determination of surface deformations, but in the last two decades more InSAR techniques have appeared chronologically systematized in Fig. 11.

Another approach of PS InSAR is the small baseline distances between either the satellite positions of different acquisition times, which is used to reduce the geometric and temporal decorrelation. This method also has time-series analysis approach and is called the small baseline subset. [11]

The major restriction of this approach is that it is limited to the scatterers that have sufficiently high coherence, even at large baselines, which typically leads to low PS density in nonurban areas. [4]

For first time this technique is developed and published in paper of Berardino et al (2002).

PSI method reference	Baseline configuration	Pixel selection criterion	Deformation model
Ferretti et al. (2000, 2001)	Single master	Amplitude dispersion	Linear deformation in time
Berardino et al. (2002)	Small baselines	Coherence	Spatial smoothness
Mora et al. (2003)	Small baselines	Coherence	Linear deformation in time
Schmidt and Bürgmann (2003)	Small baselines	Coherence	Spatial and temporal smoothness
Werner et al. (2003)	Single master	Amplitude dispersion & Spectral phase diversity	Linear deformation in time
Duro et al. (2003) and Crosetto et al. (2008)	Small baselines	Amplitude dispersion, coherence, spectral coherence	Linear deformation in time
Kampes (2006)	Single master	Amplitude dispersion & Signal to clutter ratio	Different types of deformation models
Hooper et al. (2004)	Single master	Amplitude and phase criterion	Spatial smoothness
Crosetto et al. (2005)	Small baselines	Coherence	Stepwise linear function in time
Costantini et al. (2008)	Single master	Amplitude dispersion	Linear deformation in time
López-Quiroz et al. (2009)	Small baselines	Coherence	Spatial smoothness
Ferretti et al. (2011)	Single master after triangulation	Statistical homogeneity test	Deformation model in time
Perissin and Wang (2012)	Target-dependent interferogram subset	Quasi-PS approach	Linear deformation in time
Hetland et al. (2012)	Small baselines	Coherence	Different types of deformation models
van Leijen (2014)	Single master	Amplitude dispersion	Different types of deformation models
Goel and Adam (2014)	Small baselines	Statistical homogeneity test	Linear deformation in time
Lv et al. (2014)	Single master	Statistical homogeneity test	Linear deformation in time
Devanathéry et al. (2014)	Small baselines	Amplitude dispersion & Cousin PS	Spatial smoothness

Fig.11 Characteristics of the main PSI approaches. [4]

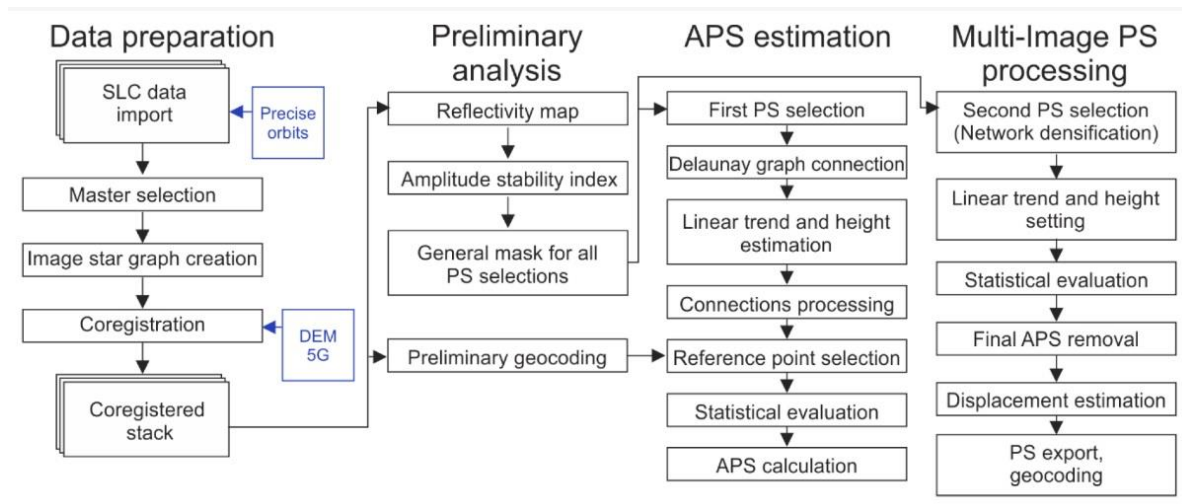


Fig.12 Simplified workflow of PSI Processing in SARPROZ [7]

PSInSAR processing is a very complex procedure that requires high knowledge and requires the use of several scientific software packages.

In the paper [7] is presented simplified workflow of PSI processing in software SARPROZ. (Fig. 11) The authors emphasized that a critical part is the coregistration of the SAR images into a single master SAR image before deriving interferograms. It is very important to choose a proper master scene which must have the following specifications:

- It must be acquired under good weather conditions (no rain) and
- That has a suitable position (approximately in the middle) in the image star graph considering the perpendicular and temporal baseline.

In the paper [12], the author used several scientific software packages, developed on different universities. Their first step in the data processing was focusing the radar image to obtain the single look complex images (SLC). For that they planned to use the scientific package ROI-PAC (Repeat Orbit Interferometry Package) developed at the Jet Propulsion Laboratory (JPL) on the Caltech (California Institute of Technology) university, but in the processing that step was skipped, because they used directly SLC radar data downloaded from ESA (European Space Agency) web side. The interferogram which they processed is generated in DORIS (Delft object-oriented radar interferometric software) developed at the TU Delft, Netherland. The phase unwrapping process, they did in SNAPHU software developed by Stanford. And the phase processing they did in scientific software StaMPS/MTI (Stanford method for persistent

Scatterer/Multi Temporal InSAR) developed at the Stanford University.

The complete processing procedure is shown in Fig. 13.

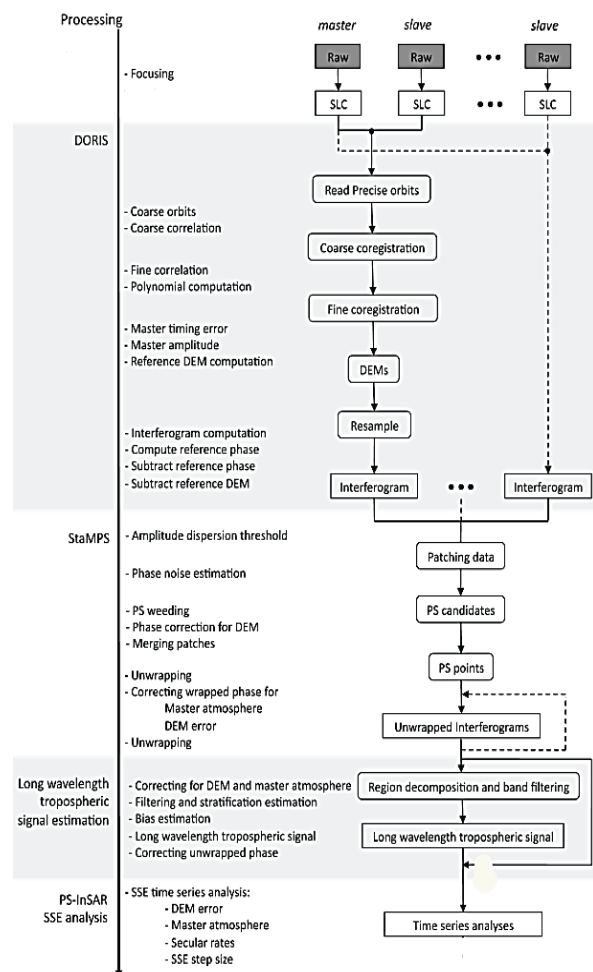


Fig.13 PSInSAR processing with using of many software packages [12]

4. CONCLUSION

InSAR technology is capable of responding to the needs for continuous and massive monitoring of the Earth's surface, through the determination of its deformations. This is proven by numerous works in the last two decades devoted to this particular issue.

In almost all studies and research on this topic, the general conclusion is that this technology offers opportunities for determining vertical deformations within a few millimeters, using the advanced PSInSAR technique. For this purpose, in many papers, comparative analyzes of this technology have been made with the classical methods for deformation analyses. In most of them, the both methodologies give the similar results.

The advantage of this technology compared to other geodetic methods for determining Earth's deformations is the possibility to use it on large areas, in any period from the past when SAR images are available.

The disadvantages of this technology are the impossibility of using it for every surface, especially surfaces with dense vegetation. Also, a disadvantage of this technology can be the complex processing of SAR images.

In general, it is a new technology that is constantly being upgraded and sets a new standard in the determination of vertical deformations.

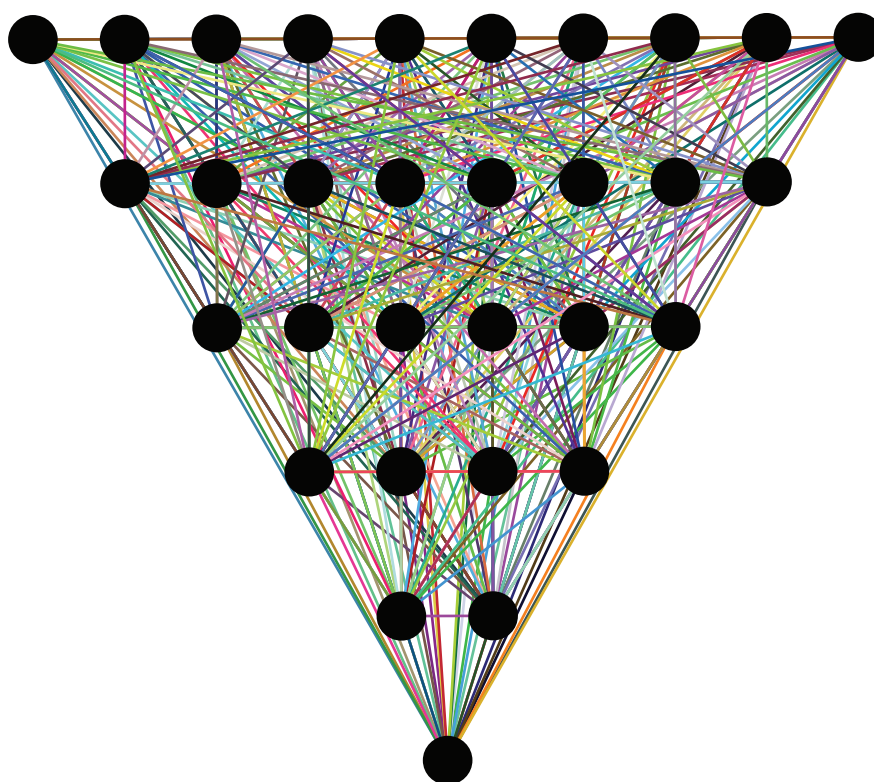
REFERENCES

- [1] Bamler, R., & Hartl, P. (1998). Synthetic aperture radar interferometry. *Inverse Probl.*
- [2] D'Hondt, O., & Hellwich, O. (2018). Regularization and Completion of TomoSAR Point Clouds in a Projected Height Map Domain. *IEEE Journal of Selected Topics in Applied Earth Observations and Remote Sensing*, 9.
- [3] Bellotti, F., Alessandro, F., & Del Conte, S. (2015). Advanced InSAR techniques to support tectonic settings analyses. *Rendiconti Online Societa Geologica Italiana*.
- [4] Crosetto, M., Monserrat, O., Cuevas-González, M., & Devanthery, N. (2016). Persistent Scatterer Interferometry: A review. *ISPRS Journal of Photogrammetry and Remote Sensing*.
- [5] EarthData. (2022). *What is Synthetic Aperture Radar*. Retrieved from <https://www.earthdata.nasa.gov/learn/backgroundunders/what-is-sar>
- [6] ESA. (2021). *TOPS Interferometry Tutorial*.
- [7] Fárová, K., Jelének, J., Kopacková-Strnadová, V., & Kycl, P. (2019). Comparing DInSAR and PSI Techniques Employed to Sentinel-1 Data to Monitor Highway Stability. *Remote sensing*.
- [8] Ferretti, A., & Rocca, F. (2000). Analysis of Permanent Scatterers in SAR interferometry. *IEEE Transactions on Geoscience and Remote Sensing*.
- [9] Hanssen, R. F. (2001). *Radar Interferometry*.
- [10] Imperatore, P., Pepe, A., & Sansosti, E. (2021). High Performance Computing in Satellite SAR Interferometry. *Remote sensing*.
- [11] Jia, H., & Liu, L. (2016). A technical review on persistent scatterer interferometry. *Journal of Modern Transportation*.
- [12] Pribicevic, B., Đapo, A., & Govorcin, M. (2018). Surface Deformation Monitoring in the Republic of Croatia with MT-InSAR.
- [13] RiskNET. (2016). *INTERFEROMETRIC SYNTHETIC*. Retrieved from An Introduction for Users of InSAR: <http://www.risknet-alcotra.org/rna/allegati/insar-manual.pdf>
- [14] TRE Altamira. (2022). *TRE Altamira*. Retrieved from InSAR at a glance: <https://site.tre-altamira.com/insar/>
- [15] Valentino, G. (2021, May 3). Introduction to Interferometric SAR - Dr. Gianluca Valentino (theory). Malta.

THE AII4R&D PLATFORM HAS PUT US ON THE MAP



WE IMPROVE THE KNOWLEDGE TRIANGLE
AND JOINTLY ACCELERATE INNOVATION



35 INNOVATIVE TEACHING PRACTICES

8 RESEARCH PROJECTS LINKED TO REAL SECTOR

50 PROFESSIONAL COURSES WITH 500 PARTICIPANTS

DIVERSE NETWORK OF 6 COUNTRIES AND 14 PARTNERS



Promoting academia-industry alliances
for R&D through collaborative and
open innovation platform - AII4R&D
www.platform.all4rd.net

Co-funded by the
Erasmus+ Programme
of the European Union



Ditar Memedi

MSc, Assistant
South East European University
Faculty of Contemporary Sciences and
Technologies Tetovo, North Macedonia
ditarm2@gmail.com

Denis Popovski

PhD, Associate Professor
Ss. Cyril and Methodius University
Faculty of Civil Engineering – Skopje
popovski@gf.ukim.edu.mk

Mile Partikov

PhD, Assistant Professor
Ss. Cyril and Methodius University
Faculty of Civil Engineering – Skopje
partikov@gf.ukim.edu.mk

Albnor Nasufi

MSc, Civ. Eng.
North Macedonia
nolinasufi@live.com

ANALYTICAL MODEL OF NON-SWAY STEEL FRAME WITH SEMI-RIGID CONNECTIONS

The distribution of moments in a steel frame is directly correlated, beside other parameters, by the rigidity of the connection between the constituent elements. Depending on the type of beam-column connection, i.e. depending on its initial rotational stiffness, a diagram of internal static quantities is also generated. In design practice, the traditional way of treating a beam-column connection is carried out by assuming one (or their mutual combination) of the following ideal cases:

1. Absolute rigid connection
2. Absolute pinned connection

This of course, misinterprets the actual behavior of the structure and contributes to unnecessary increased material consumption

The real rigidity of a connection is always between these two extremes cases. Eurocode 3, Part 1-8 provides rules and procedures for quantifying the initial rotational stiffness of a bare steel connection, but does not specify how to determine the moment in the connection joint from the influence of given external loads.

The purpose of this paper is to describe the distribution of moments in a non-sway steel frame with semi-rigid connections under the influence of a uniformly distributed vertical loads and to answer the following question:

Is it more convenient to analyze the beam as an isolated element with semi-rigid connections at the ends or is it necessary to include the rigidity of the vertical elements (columns)?

This goal has been achieved by proposing a two-parameter analytical model that includes both the rigidity of the columns and the rotational rigidity of end beam connections, all together included in one model. The proposed model is compared to the Liu and Chen model [3] which gives the dependence between the external load and the negative moment in the semi-rigid connection, taking into account only the initial rigidity of the beam-column connection.

According to this model for determining the distribution of moments, the rigidity of the vertical construction – columns is neglected. This way of neglecting the columns in analysis

of a steel frame is also adopted in Eurocode 3, Part 1-8.

This of course contributes to the slight overestimation of the negative moment in the beam-column relationship. Determination of the moment in the sagging and hogging region (connection node) from a given external uniformly distributed vertical load is directly dependent on the rotational rigidity of the connection (secant stiffness, S_j) and the rigidity of the vertical structure (k_c).

Keywords: semi-rigid connections, beam-column connection, rotational stiffness, column stiffness, steel frames.

1. PROPOSED TWO-PARAMETER MODEL

The construction of the model starts with the consideration of a bare steel frame with span L_b . The height of floor 1 and floor 2 are h_1 and h_2 respectively (Figure (1)).

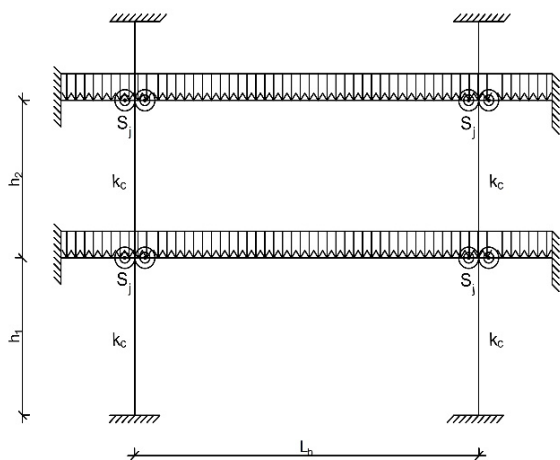


Figure 1. Non-sway bare steel frame with semi-rigid connections

The stiffness of the column beam connection is denoted by $S_{j,ini}$, while the stiffness resulting from the columns is denoted by k_c . To explain the mechanism of transfer of the moment from the beam to the beam-column connection, including column rigidity, an isolated beam is considered as an integral part of the frame, shown in Figure (2).

The correlation between the rigidity of the columns and the rigidity of the beam-column

connection is taken as an integral part in the node itself, it is shown in Figure 2 a). The total stiffness that comes from k_c and S_j is denoted by k and is determined by the equation([4]):

$$\frac{1}{k} = \frac{1}{k_c} + \frac{1}{S_j} \quad (1)$$

Or, equivalently:

$$k = \frac{k_c S_j}{k_c + S_j} \quad (2)$$

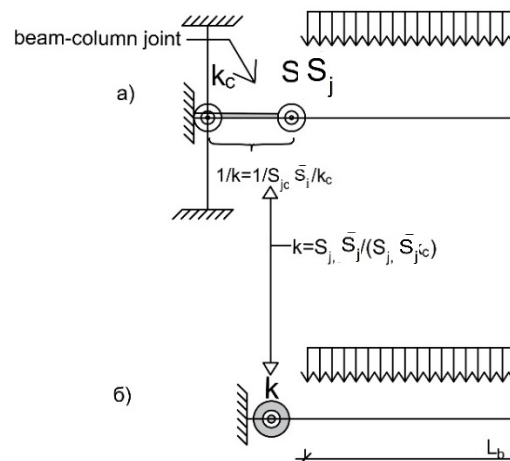


Figure 2. a) Effect of column on beam-column connection b) combining column rigidity k_c and connection stiffness

The parameter k is the parameter "S_j" for the isolated beam, if it is treated according to the philosophy adopted in Eurocode 3, Part 1-8. In addition, the mechanism of transfer of bending moments from the beam to the connection node is shown, with taking into account the above functional parameters. The bending moment at the connection node is related to the relative rotation between the beam-column. The problem is solved in stages:

1.1 ROTATION - STAGE I

In the first stage, the rotation of a simple supporting beam is determined depending on the intensity of the vertical external load according to the expression:

$$\theta_0 = \frac{qL_b^3}{24EI_b} \quad (3)$$

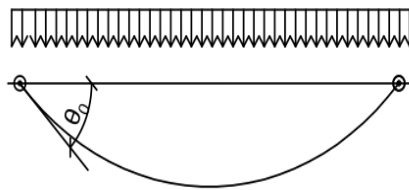


Figure 3. Positive rotation of simply supported beam

1.2 ROTATION - STAGE II

In the second phase, two sub-phases are considered:

- Negative end beam rotation with semi-rigid connection (S_j)

Depending on the external uniformly distributed vertical load and the unknown amount of bending moment (M_{ed} -which is to be determined by this procedure) that appears in the beam-column connection, the "negative" end beam rotation by including these effects is expressed by:

$$\theta_{sr} = \frac{M_{ed}}{2EI_b} \quad (4)$$

- Negative beam rotation due to the rigidity of the column (k_c)

The relationship between the Negative rotation, the unknown moment in the node (M_{ed}) of the connection and the rigidity of the vertical structure that occurs due to the rigid effects of the column is determined by the following relation:

$$\theta_{kc} = \frac{M_{ed}}{k_c} \quad (5)$$

where k_c is calculated by([5]):

$$k_c = \frac{\alpha_1 E_s I_{c1}}{h_1} + \frac{\alpha_2 E_s I_{c2}}{h_2} \quad (6)$$

- h_1 –story height for level 1,
- h_2 –story height for level 2 и
- the modulus of elasticity of the columns in the corresponding positions. The coefficient α_1 for columns fixed in the base is 4. If the columns are pinned to the base, then the value of the coefficient is $\alpha_1 = 3$ while the coefficient α_2 , would always have the value $\alpha_2 = 4$.

Together with the above-mentioned, by adopting the principle of superposition of influences, these two sub-mechanisms are combined as shown in the following sketch:

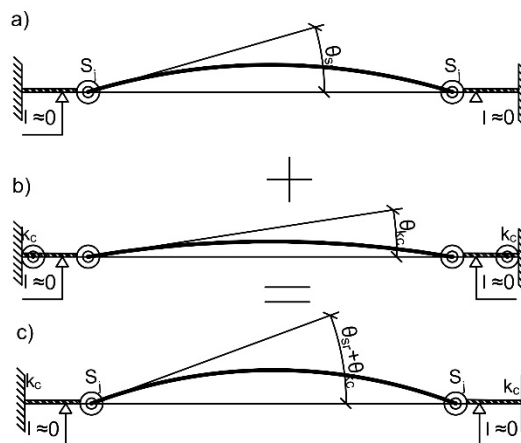


Figure 4. a) Negative rotation due to beam-column stiffness b) Negative rotation due to column rigidity c) Overall negative rotation from last two effects

The sum of the positive rotation of simply supported beam and the last two „negative” rotations (based on Figure 4c) is:

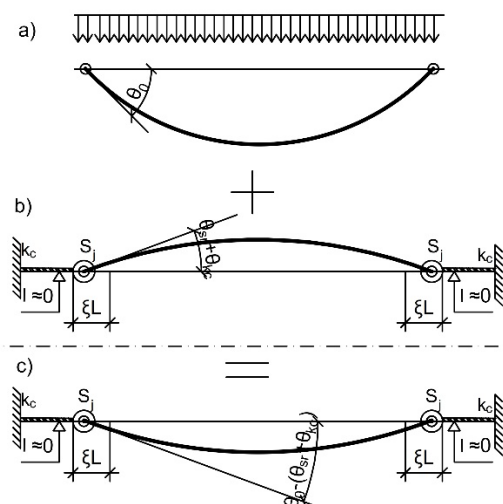


Figure 5. a) Positive rotation due to stage I b) Negative rotation due to stage II c) Overall positive rotation due to combined effects

The last one (Figure 5c), mathematically is represented by:

$$\theta_{S_j} = \theta_0 - (\theta_{sr} + \theta_{kc}) \quad (7)$$

$$= \frac{ql^3}{24EI_b} - \left(\frac{M_{ed}}{2EI_b} + \frac{M_{ed}}{k_c} \right)$$

Where θ_0 , θ_{sr} and θ_{kc} denote the rotation of a simple beam, the negative rotation due to the semi-rigid effects at the end beam and the negative rotation due to the rigidity of the columns, respectively.

The correlation between the external load moment (M_{ed}) and the corresponding secant

stiffness S_j is given by the well-known expression:

$$\theta_{S_j} = \frac{M_{ed}}{S_j} \quad (8)$$

By equalizing expressions (7) and (8), the hogging moment of the external load at the column-beam connection can be represented as follow:

$$\frac{M_{ed}}{S_j} = \frac{ql^3}{24EI_b} - \left(\frac{M_{ed}}{2EI_b} + \frac{M_{ed}}{k_c} \right) \quad (9)$$

Expressing M_{ed} from (9) gives:

$$M_{ed} = \frac{ql_b^3}{24EI_b} \frac{1}{\left(\frac{1}{S_{j,c}} + \frac{1}{k_c} + \frac{L_b}{2EI_b} \right)} \quad (10)$$

Equation (10) can be transformed into the following form:

$$M_{ed} = \frac{\frac{ql_b^3}{24EI_b}}{\frac{L_b}{EI_b} \left(\frac{EI_b}{S_{j,c}L_b} + \frac{EI_b}{k_cL_b} + \frac{1}{2} \right)} \quad (11)$$

If $\frac{S_{j,c}L_b}{EI_b}$ and $\frac{k_cL_b}{EI_b}$ are denoted by R_1 and R_2 , respectively, then the last expression would take the final form:

$$M_{ed} = \frac{2R_1R_2}{3(2R_1+2R_2+R_1R_2)} \cdot M_{sag}^0 \quad (12)$$

The proposed two parameter model (12) incorporates the parameters R_1 and R_2 and the sagging bending moment M_{sag}^0 if the beam is considered as a simply supported beam. That is, the moment of the external load in the connection node is given as a functional dependence on the following parameters:

$$M_{ed} = M_{ed}(M_{sag}, S_j, k_c) \quad (13)$$

The coefficient $\frac{2R_1R_2}{3(2R_1+2R_2+R_1R_2)}$ is always a number less than 1. In other words, this quotient is a reduction of the sagging moments of a simply supported beam and the same reduction is transmitted from region of positive moment to the node of the semi-rigid beam-column connection.

2. DESCRIPTION OF ONE-PARAMETER MODEL ACORDING TO LIU AND CHEN

As a comparison, if we do not take into account the participation of the vertical construction then a change in the law of moments instead of a two-parameter function (12) would be described using a graph of a function of one main variable (S_j). That's only with one parameter i.e. the parameter R_1 . The next paragraph describes the philosophy of this approach.

The total end beam rotation is assumed to be the sum of the rotation when the beam is considered to be simply supported by a uniformly distributed load and the "negative" rotation when the beam is exposed to a negative moment due to the semi-rigid effect that causes the beam to "overhang".

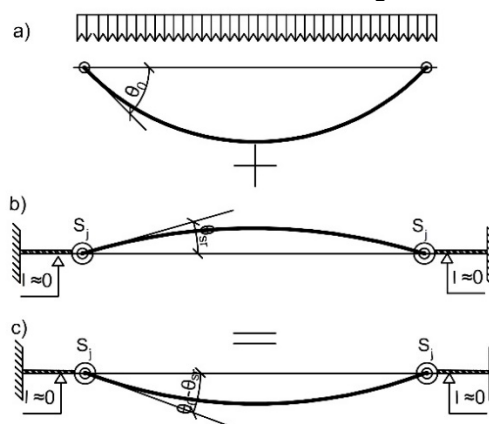


Figure 6. a) Positive rotation due to stage I b) Negative rotation due to beam-column rotational stiffness c) Overall positive rotation due to combined effects

Where:

- θ_0 : Rotation of a simply supporting beam by the action of an uniformly distributed vertical load
- θ_{sr} : Negative rotation due to the effect of a semi-rigid connections
- S_j : Secant rigidity of bare steel semi-rigid connection

In this model, it is evident that the columns do not participate in the distribution of moments. As in previous model, the superposition principle is assumed so the total rotation of the end beam node can be defined as:

$$\theta_j = \theta_0 - \theta_{sr} \quad (14)$$

$$\theta_0 = \frac{ql_b^3}{24EI_b} \quad (15)$$

$$\theta_{sr} = \frac{ML_b}{2EI_b} \quad (16)$$

By substituting equations (16) and (15) in equation (14) we get:

$$\theta_j = \frac{qL_b^3}{24EI_b} - \frac{M_{ed}L_b}{2EI_b} \quad (17)$$

By equalizing equations (17) and (8), the moment in the semi-rigid connection node is determined according to the relation:

$$M_{ed} = \frac{2R_1}{3(R_1+2)} M_{sag}^0 \quad (18)$$

Where:

- R_1 : coefficient of rotational stiffness which is $R_1 = \frac{S_{j,c}L_b}{EI_b}$.
- M_{sag}^0 : The moment in sagging region when the beam is treated as simply supported.

3. COMPRAISON OF THE PROPOSED MODEL WITH THE ONE PARAMETRIC MODEL

To have a better understanding on differences between the proposed model and the standard one parametric model [3], the following example is considered:

A bare steel frame with two stories under the influence of uniformly distributed vertical load of $g_{ed} = 12.5 \text{ kNm}$ is considered. The columns are selected as HEB160 with height of $h_1 = 4\text{m}$ and $h_2 = 3\text{m}$. The beam is selected as IPE240 with span $L_b = 8\text{m}$.

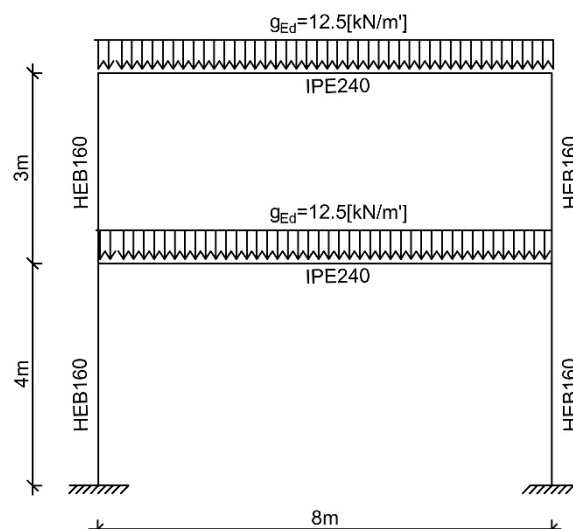


Figure 7. a) Positive rotation due to stage I b) Negative rotation due to beam-column rotational stiffness c) Overall positive rotation due to combined effects

The initial rotational stiffness and the secant stiffness of the beam-column connection calculated in [5] are: 8816 kNm/rad and 4408 kNm/rad, respectively. With the implementation of the proposed method, the moment in the connection node (M_{hog}) as well as sagging moment (M_{sag}) for the first story are determined by calculating all the necessary parameters. The results for the proposed model are shown in the table below.

Table 1. Calculation according to the proposed model

Parameter	Calculated parameters
$S_{j,ini}$	8816 kNm/rad
S_j	4408 kNm/rad
R_1	4.31
k_c	12210.8 kNm
R_2	11.92
$\frac{2R_1R_2}{3(2R_1 + 2R_2 + R_1R_2)}$	0.4
M_{sag}^0	100 kNm
M_{hog}	40 kNm
M_{sag}	60 kNm

From the shown table calculations, it is noticed that the positive bending moment, M_{sag} , is 60 kNm

In the following table, the calculation of the positive moments, M_{sag} , for the same example

was carried out, but with the implementation of the one-parameter model.

Table 2. Calculation according to the one-parameter model

Parameter	Calculation of parameters
$S_{j,ini}$	8816 kNm/rad
S_j	4408 kNm/rad
R_1	4.31
$\frac{2R_1}{3(R_1 + 2)}$	0.46
M_{sag}^0	100 kNm
M_{hog}	46 kNm
M_{sag}	54 kNm

From the performed analysis, it is noticed that, for the same frame and the same level of loads, the positive moment for the first story is 54 kNm.

A comparison of the obtained results is described in the following sketch:

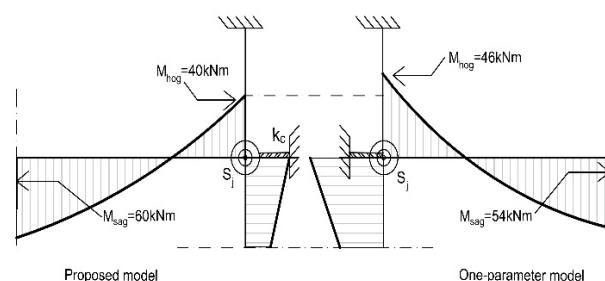


Figure 8. Hogging and sagging moments calculated by proposed model and their comparison with moments calculated by one-parameter model.

4. CONCLUSION

This paper presents a two-parameter analytical model for determining the negative moment in a semi-rigid bare steel, beam to column connection.

In this model, in addition to the secant rigidity of the beam-column connection, the rigidity of the vertical construction is considered through the parameter k_c . The purpose behind the introduction of this parameter was to assess whether the neglect of the column rigidity has a favorable or unfavorable effect on the distribution of moments in a bare steel frame.

Next, a one parameter model based on Liu and Chen([3]) is presented and their mechanism of transferring the bending moment in a bare steel frame is compared.

The reason for this comparison (with a one-parameter model) is precisely due to the fact that the philosophy of dealing with this issue in Eurocode 3 is based on this one-parameter model.

From the conducted analysis, with the two-parameter model, for the same frame and the same level of loads, the sagging moment is approximately 10% higher compared to the one-parameter model.

As a final conclusion can be drawn that, analysing a beam as an isolated beam with semi-rigid connections and excluding column rigidity implies underestimating sagging moment and overestimating the hogging moments.

REFERENCES

- [1] EN 1991-1-1: Eurocode 3: Design of steel structures – Part 1-1: General rules and rules for buildings, CEN 2005.
- [2] EN 1991-1-8: Eurocode 3: Design of steel structures – Part 1-8: Design of joints, CEN 2005.
- [3] Chen, W. F. and Lui, E. M. „Stability design of steel frames“ CRC Press, 1991. Eurocode - Basis of structural design
- [4] Faella, C., Piluso, V., and Rizzano, G., „Structural steel semi-rigid connections— Theory, design and software“, CRC Press, Boca Raton, FL, 2000.
- [5] Y.L. Wong, T. Yu, S.L. Chan. „A simplified analytical method for unbraced composite frames with semi-rigid connections“, Journal of Constructional Steel Research, 63 (2007)
- [6] М. Дитар: „Анализа на спрегнати рамки со полукрути спрегнати врски“(Master Thesis, 2022)

Viktor Mickovski

Acoustics Consultant
M-Akustik
viktormickovski@gmail.com

Gino Iannace

PhD, Professor
Università della Campania 'Luigi Vanvitelli'
Department of Architecture and Industrial
Design – Aversa, Italy
gino.iannace@unicampania.it

Milica Jovanoska-Mitrevska

MSc, Teaching Assistant
Ss. Cyril and Methodius University
Faculty of Civil Engineering – Skopje
m.jovanoska@gf.ukim.edu.mk

Todorka Samardzioska

PhD, Professor
Ss. Cyril and Methodius University
Faculty of Civil Engineering – Skopje
samardzioska@gf.ukim.edu.mk

REBONDED POLYURETHANE FLEXIBLE FOAM AS SOUND ABSORBING MATERIAL

Polyurethane (PU) foams are highly established material in noise control engineering, but also in other remarkably versatile domains. Unfortunately, this increases the amount of PU waste disposal in the landfills. Concerning the new strategies for sustainable and green polyurethanes, this study investigates the sound absorption properties of Rebonded PolyUrethane (RPU) foam.

Measurements of sound absorption coefficient, α , under normal incidence were made using an impedance (Kundt) tube for RPU foam samples with two different densities ($40 \text{ kg/m}^3 \pm 15\%$ and $60 \text{ kg/m}^3 \pm 15\%$) and three different thicknesses (45 mm, 70 mm and 95 mm). The airflow resistivity was also measured for the same samples.

The Transfer Matrix Method (TMM) was employed to simulate the sound absorption phenomenon for normal and diffuse sound incidence of unbounded poro-elastic RPU layer with hard wall termination. The visco-inertial dissipative effects inside the porous layer were described with Johnson-Champoux-Allard (JCA) model.

Keywords: sound absorption coefficient, airflow resistivity, impedance tube, transfer matrix method, rebonded polyurethane foam

1. INTRODUCTION

Polyurethane production reached a total of 22.3 million tons and grew at a rate of 4.0 % during 2016, while the estimated global polyurethane production for 2020 was 28.2 million tons, with an annual production growth rate of 5,2 % [1]. PU production is constantly increasing due to their diverse application, which leads to an increase in the amount of polyurethane waste in the environment.

Polyurethanes are group of polymers, produced using petroleum-based polyols and diisocyanate and they are generally very resistant to biodegradation. The methods for PU recycling can be categorized into three groups: mechanical recycling, chemical recycling and energy recovery. Mechanical

recycling consists of grinding/shredding the polyurethane waste and then, reprocessing. With chemical recycling the PU is chemically degraded, while energy recovery considers combustion of polyurethane foam waste to recover energy. Regarding costs, applied temperature and additional substrates, chemical recycling is very demanding process and only two chemical recycling methods are implemented on a large scale (glycolysis and gasification), while others are still in the research stage, [2]. Mechanical recycling is, so far, the most effective and economic route for recycling.

Flexible and rigid foams are the two main types of polyurethanes. Rebonded PU foams are mechanically recycled polyurethane foams, manufactured from grinded foam, pressed and bonded with binder. Rebonded polyurethane foam is a very convenient way to reuse PU foam waste.

There are many research studies dedicated to acoustic characterization of PU foams, but there is a vast research area for the recycled PU foams that has yet to be addressed. Del Rey et al., [3], [4], studied the acoustic properties of recycled foams developed from grinded polyurethane foam waste with different internal composition. Tiuc et al., [5], research the sound absorption of recycled PU foams developed by using grinded rigid PU foam waste as a raw material. Sabbagh and Elkhateeb, [6], investigate the absorption coefficients of rebonded PU foam in the reverberation chamber. Bougdah and Hall, [7], performed field measurements and Nering et al., [8], measured the dynamic stiffness, and critical damping coefficient in order to investigate the possibility of using rebonded PU foam for impact sound insulation. Parikh et al., [9], study the absorption properties of rebonded polyurethane foam and possibility to use it as underpad for reduction of automotive interior noise.

Despite the fact that rebonded PU has been used for a long time, its potential has not been extensively explored. Therefore, this paper focuses on acoustic characterization of rebonded PU flexible foams with different densities and thicknesses. Sound absorption coefficients are measured using impedance tube and airflow resistivity is also measured for the same specimens. Based on the obtained experimental results, transfer matrix method was employed for extended research.

2. MATERIALS & METHODS

Rebonded polyurethane foam specimens were produced from shredded polyurethane waste combined with binder and then exposed to pressure. This type of mechanical recycling technology creates non-homogenous distribution of the volume weight in the produced foam block. Specification of the volume weight is based on measuring and weighing the entire block.

Two different densities were produced by a local PU flexible foam manufacturer: $40 \text{ kg/m}^3 \pm 15\%$ and $60 \text{ kg/m}^3 \pm 15\%$, Figure 1. For each density, 3x3 cylindrical samples with thicknesses: 45 mm, 70 mm and 95 mm, were cut out, each with diameter of 100 mm.



Figure 1. Rebonded polyurethane foam specimens: a) $\rho=40 \text{ kg/m}^3$, b) $\rho=60 \text{ kg/m}^3$

For acoustic characterization of the RPU foam, airflow and impedance (Kundt) tube measurements were performed on the same samples. From the measurements, the airflow resistivity, R_1 , and the sound absorption coefficients, α , were obtained. The measurements were conducted in the

laboratory facilities of University of Campania "Luigi Vanvitelli", Department of Architecture and Industrial design.

The airflow resistivity (flow resistance per unit thickness) is very important acoustic parameter that is associated with the absorption capacity of the material. For the selected rebonded foam specimens, the airflow resistivity was measured according the ISO 9053, [10], following the alternating airflow method, using the measuring device SCS9023, Figure 2, [11]. The airflow resistivity, R_1 , is obtained from Equation 1, under alternate air flow generated with a piston at a frequency of 2.0 Hz.

$$R_1 = \frac{\Delta p}{v \cdot \Delta x} \text{ [Rayl/m]} \quad (1)$$

where Δp is pressure difference, v is air velocity and Δx is the thickness of the specimen, in the direction of the flow, in metres.



Figure 2. Airflow resistivity measuring device SCS9023

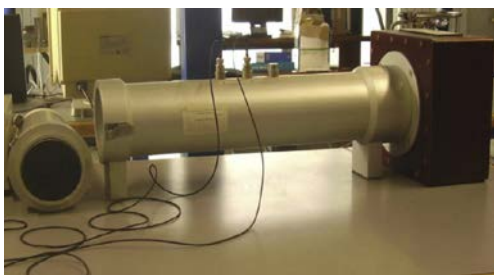


Figure 3. Impedance tube SCS9020

The normal incidence sound absorption coefficients of the RPU specimens were measured with SCS9020 impedance (Kundt) tube, Figure 3, [11], in accordance with ISO 10534-2, [12].

On the one end of the tube there is a noise source that generates plane waves and on the other end, the test sample is mounted. The impedance tube has internal diameter of 100 mm and length of 570 mm and provides satisfactory results for the absorption

coefficients in the frequency range 250 Hz – 2000 Hz. The sound absorption coefficients are obtained from the acoustic transfer functions measured with the two microphones.

By using the transfer matrix method, unbounded poro-elastic layer with hard wall termination on one side and semi-infinite fluid on the other side was modeled, considering plane wave propagation, Figure 4.

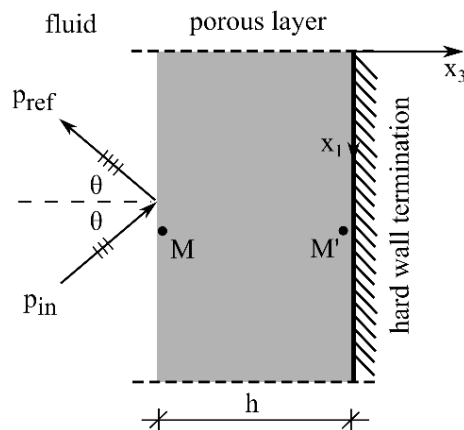


Figure 4. Unbounded poro-elastic layer backed with hard wall for transfer matrix calculation

Transfer matrix method is simple but powerful method widely used in many fields of physics among which the field of acoustics. It is used to calculate the wave propagation in a layered system where each layer within the system is defined by a transfer matrix. The size of the matrix depends on the type of the layer. For elastic-solid layer is 4x4, for elastic-porous layer is 6x6, for stationary fluid layer is 4x4 etc., [13]. This depends on the number of quantities that describe the acoustic field in the layer. For example, for a porous layer, 6 quantities describe the acoustic field: two velocity components of the porous frame (v_1 and v_3), one velocity component of the fluid (v_3), two components of the stress tensor of the porous frame (σ_{33} and σ_{13}) and one in the fluid (σ_{33}). The surface impedance, Z_s , is obtained directly from the transfer matrix for given boundary conditions. Hence, reflection, absorption, transmission and other phenomena can be easily studied.

The transfer matrices relate the variables V that describes the acoustic field of the medium on both sides:

$$V(M) = [T]V(M') \quad (2)$$

where M and M' are points near the forward and backward face of the layer.

The considered porous layer, on one side, interacts with semi-infinite fluid so the continuity

condition for fluid-porous interface was applied. On the other side, hard wall termination condition was imposed (infinite impedance). Next, the surface impedance of the medium is determined, the reflection coefficient and then the absorption coefficient.

The visco-inertial and thermal dissipative effects occurring in the porous medium were described with Johnson-Champoux-Allard (JCA) model. For this model, besides air flow resistivity R_1 , that is measured, several other parameters are needed: porosity ϕ , tortuosity a_∞ , viscous characteristic length Λ and thermal characteristic length, for which the following dependency is adopted: $\Lambda' = 2\Lambda$. Porosity is estimated from the Equation 3, while the other parameters are obtained by fitting the measured curves. Same values per density were adopted.

$$\phi = 1 - \frac{\rho_{bulk}}{\rho_{solid}} \tag{3}$$

After obtaining the intrinsic parameters for the two densities, the sound absorption coefficient for diffuse sound incidence was calculated with TMM through integration:

$$\alpha_{diff} = \int_0^{\pi/2} \alpha(\theta) \sin 2\theta d\theta \tag{4}$$

The Noise Reduction Coefficient, NRC , was also calculated. NRC is a single-number rating of sound absorption and is widely used as a parameter to characterize and compare sound-absorbing materials. NRC is the arithmetic mean of the absorption coefficients for 250 Hz, 500 Hz, 1000 Hz, 2000 Hz, [14]:

$$NRC = \frac{\alpha_{250} + \alpha_{500} + \alpha_{1000} + \alpha_{2000}}{4} \tag{5}$$

3. ANALYSIS & RESULTS

The measured airflow resistivity for the two considered densities are shown in Table 1. The airflow resistivity influences the sound absorption properties and is one of the parameters of the JCA model.

Table 1. Airflow resistivity

Density [kg/m ³]	R ₁ [Rayl/m]
40	3800
60	5000

The normal incidence sound absorption coefficients measured with the impedance tube are presented in Figure 5. It can be seen that by increasing the thickness the low to mid

frequency absorption coefficients are improved. For example, for 500 Hz and $\rho = 40 \text{ kg/m}^3$ the absorption coefficient increases for 81% when increasing the thickness from 45 mm to 70 mm, and 43% when increasing the thickness from 70 mm to 95 mm. For 500 Hz and $\rho = 60 \text{ kg/m}^3$, the absorption coefficient increases for 76% when increasing the thickness from 45 mm to 70 mm, and 23% when increasing the thickness from 70 mm to 95 mm. As expected, the efficiency of the RPU foams for high frequencies is significant i.e., $\alpha > 0.7$.

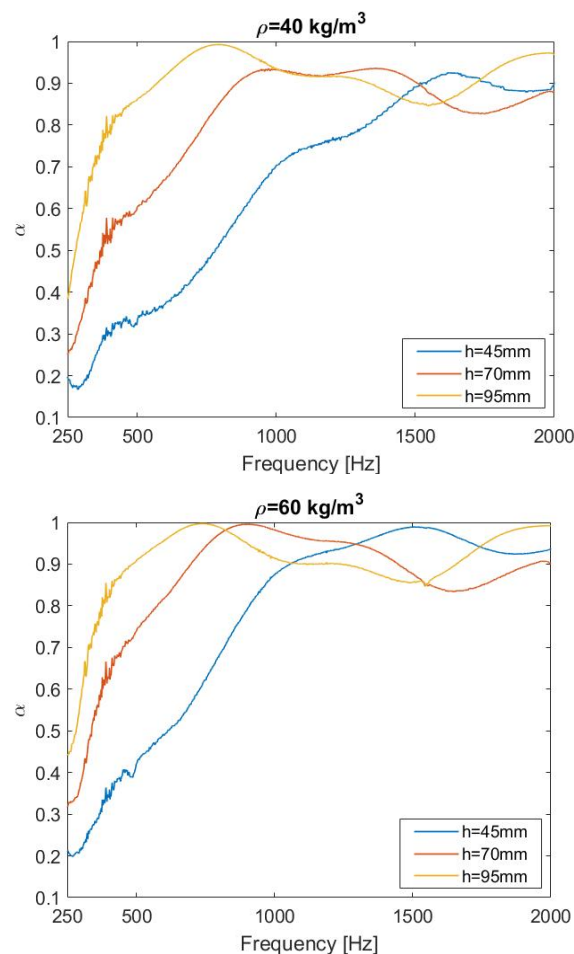


Figure 5. Sound absorption coefficients measured in impedance tube

For normal incidence, $\theta = 0^\circ$, the comparison between the experimental results and transfer matrix method is shown in Figure 6. The predicted result compares well with the experimental results with expected small discrepancies. One of the main reasons for the differences is the inhomogeneity and anisotropy of the RPU foam. Furthermore, the experimental testing was performed on samples with finite dimensions, while the calculation is based on infinite models. Also, the diffraction at the edges of finite porous samples causes constructive as well as destructive interference, [15].

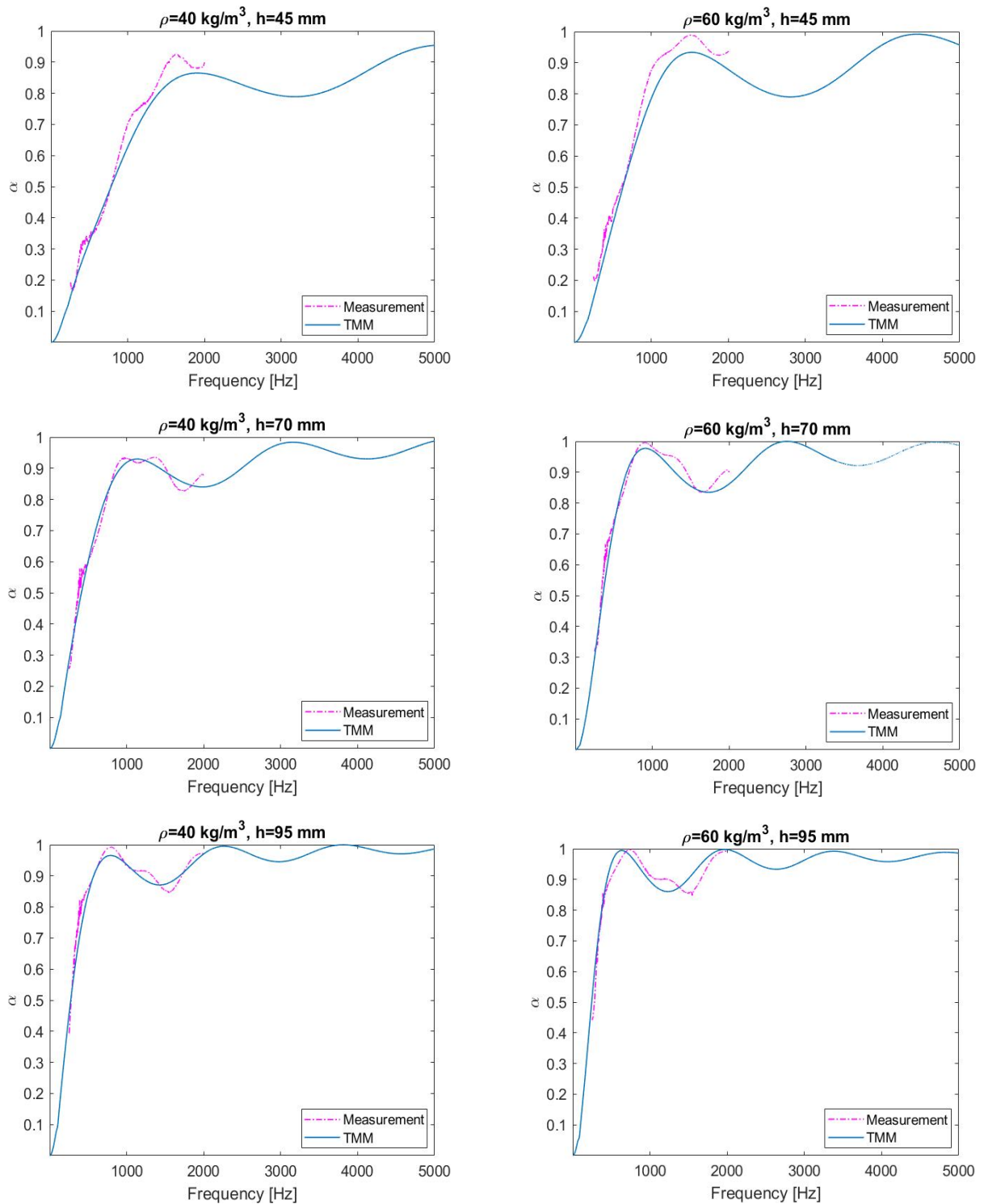


Figure 6. Sound absorption coefficients for normal incidence, $\theta=0^\circ$

By using the transfer matrix method and estimated parameters from the measurements, the sound absorption coefficients for diffuse sound field are predicted. The results are shown in Figure 7. The calculated sound absorption coefficients for diffuse sound incidence are higher for low to medium frequencies than the one for normal incidence while in the high frequency region, the diffuse sound absorption curve is smoother.

The Noise Reduction Coefficient, *NRC*, for the calculated and experimentally obtained sound absorption coefficients are shown in Table 2. The calculated *NRC* values for $\theta=0^\circ$ are close to the one obtained with measurements. The differences between the experiment and TMM simulation for *NRC* is in the range 1-10%. It can be seen that with increasing the thickness, *NRC* also increases. The same applies for the density, the specimens with higher density

perform better. The obtained values for NRC for the diffuse sound field are higher than for normal incidence, except for $\rho=40 \text{ kg/m}^3$ and $h=45 \text{ mm}$. *NRC* value of 0.70 and above is considered as good sound absorption. For the diffuse field calculation, *NRC* above 0.7, can be achieved with the thicknesses 70 mm and 95 mm.

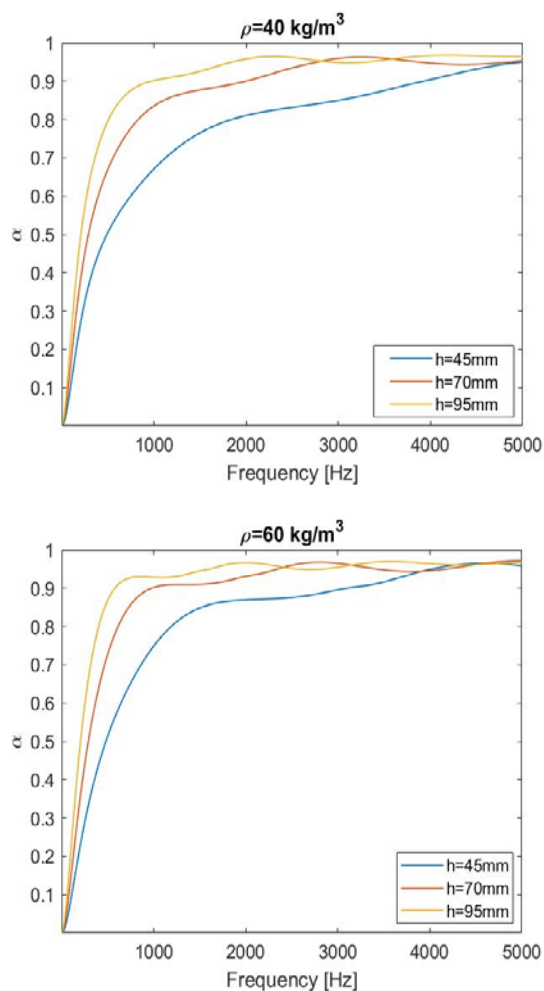


Figure 7. Absorption coefficients calculated with transfer matrix method for diffuse sound field

Table 2. *NRC* for the RPU foams

Density [kg/m ³]	<i>h</i> [mm]	<i>NRC</i>	<i>NRC</i>	<i>NRC</i>
		Exp $\theta=0^\circ$	Calc $\theta=0^\circ$	Calc diff
40	45	0.53	0.49	0.58
40	70	0.67	0.66	0.71
40	95	0.79	0.80	0.81
60	45	0.61	0.55	0.60
60	70	0.73	0.72	0.75
60	95	0.81	0.84	0.84

4. CONCLUSIONS

From the obtained results it can be seen that for RPU foams *NRC* values greater than 0.7 can be achieved. Regarding the low frequencies, which are usually a challenge when designing acoustic treatments, adequate absorption can be obtained by choosing appropriate thickness and density.

Although there are materials and products on the market with better absorption abilities, rebonded polyurethane foams, with their price and with their good relationship with the environment can be one possible solution for various noise treatment applications. One of the main challenges is to achieve a reliable and stable production process of elements with, as much as possible, uniform characteristics.

Acknowledgements

This work is a part of a co-financed project Development and production of rubber-steel elements and products from recycled polyurethane foam for protection against noise and vibration in collaboration with FITR - Fund for Innovation and Technology Development of R. Macedonia.

REFERENCES

- [1] A. Austin, D. A. Hicks, A review of the global PU industry in 2016 and outlook for 2017". PU Magazine Gupta Verlag Vol 14, Feb. 2017.
- [2] A. Kemon, M. Piotrowska, Polyurethane Recycling and Disposal: Methods and Prospects, *Polymers* 2020, 12, 1752; doi:10.3390/polym12081752
- [3] R. Del Rey, J. Alba, J. P. Arenas, V. J. Sanchis, An empirical modelling of porous sound absorbing materials made of recycled foam, *Applied Acoustics* 73 (2012) 604–609, doi: 10.1016/j.apacoust.2011.12.009.
- [4] R. Del Rey, J. Alba, J. P. Arenas, V. Sanchis, Sound absorbing materials made of recycled polyurethane foam, *Intrenoise 2011*, Osaka, Japan.
- [5] A. Tiuc, O. Nemes, H. Vermesan, D. R. Tamas-Gavrea, New Sound Absorbing Materials Obtained from Waste Rigid Polyurethane Foam, *MATERIALE PLASTICE* 56 no. 4, 2019.
- [6] M. Sabbagh, A. Elkhateeb, Sound Absorption Characteristics of Polyurethane and Polystyrene Foams as Inexpensive Acoustic Treatments, *Acoustics Australia*, 2019, https://doi.org/10.1007/s40857-019-00168-z.
- [7] H. Bougdah, R. Hall, Impact Sound Insulation of Floors Using Recycled Polyurethane Foam, Conference: *Clima 2000*, 1997, Brussels.

- [8] K. Nering, A. Kowalska-Koczwara, Determination of Vibroacoustic Parameters of Polyurethane Mats for Residential Building Purposes, *Polymers* 2022, 14, 314, doi: 10.3390/polym14020314.
- [9] D. V. Parikh, Y. Chen, L. Sun, Reducing Automotive Interior Noise with Natural Fiber Nonwoven Floor Covering Systems, *Textile Research Journal* Vol 76(11): 813–820, 2006, DOI: 10.1177/0040517506063393.
- [10] ISO 9053, Acoustics e Materials for Acoustical Applications - Determination of Airflow Resistance, 1991.
- [11] U. Berardi, G. Iannace, Acoustic characterization of natural fibers for sound absorption applications, *Building and Environment*, Volume 94, Part 2, December 2015, Pages 840-852, doi: 10.1016/j.buildenv.2015.05.029.
- [12] ISO 10534-2 (2001), Acoustics - Determination of sound absorption coefficient and impedance in impedance tubes - Part 2: Transfer-function method.
- [13] J. F. Allard, N. Atalla: *Propagation of Sound in Porous Media*, 2009, Wiley, ISBN 978-0-470-746615-0.
- [14] D. G. K. Dissanayake, D. U. Weerasinghe, L. M. Thebuwanage, U. A. A. N. Bandara, An environmentally friendly sound insulation material from post-industrial textile waste and natural rubber, *Journal of Building Engineering*, Volume 33, January 2021, 101606, doi: 10.1016/j.jobbe.2020.101606.
- [15] M. Muller-Giebeler, M. Vorlander, Modeling the edge effect for inverse determination of porous absorbers using feed forward neural networks, *Euronoise 2021*, Madeira, Portugal.



MACEDONIAN TEAM IN THE BUNDESLIGA

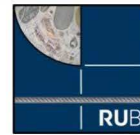


Chair of concrete and timber structures

BE PART OF THE TEAM!



Joint activities in research projects, international conferences and publication of journal papers



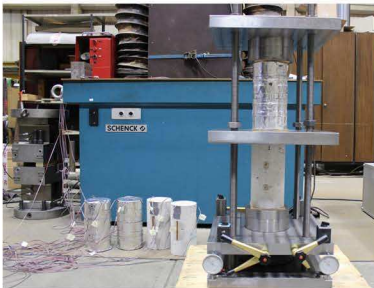
CONCRETE STRUCTURES

Prof. Dr.-Ing. habil. P. Mark



RUB
RESEARCH SCHOOL

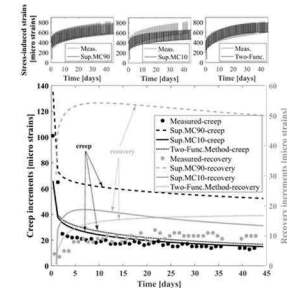
Scholarships for our young researchers provided by the RUB Research School, Germany



Experimental investigation of concrete creep and creep-recovery phenomenon, Structural testing laboratory KIBKON, RUB-Germany



Long-term experiments on reinforced concrete elements subjected to real load histories, Laboratory for concrete and structures, FCE-Skopje



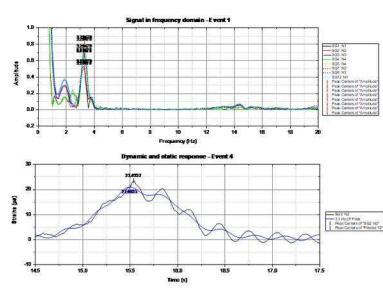
Analytical models for prediction of long-term deformations of concrete elements



Static and dynamic proof loading tests on roadway concrete bridges



Measurements of strains and deflections during the proof loading tests of concrete bridges



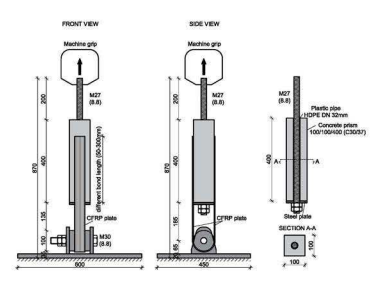
Determination of dynamic amplification factor (DAF) using Fast Fourier Transform and low-pass filtering



Time-dependent behavior of rc elements under sustained loads with various intensity, Laboratory for concrete and structures, FCE-Skopje



Long-term experiments on reinforced concrete elements strengthened by carbon strips, Laboratory for concrete and structures, FCE-Skopje



Short-term tests of concrete-carbon strips bond, Structural testing laboratory KIBKON, RUB-Germany

Albnor Nasufi

MSc, Civ. Eng.
North Macedonia
nolinasufi@live.com

Denis Popovski

PhD, Associate Professor
Ss. Cyril and Methodius University
Faculty of Civil Engineering – Skopje
popovski@gf.ukim.edu.mk

Mile Partikov

PhD, Assistant Professor
Ss. Cyril and Methodius University
Faculty of Civil Engineering – Skopje
partikov@gf.ukim.edu.mk

Ditar Memedi

MSc, Assistant
South East European University
Faculty of Contemporary Sciences and
Technologies Tetovo, North Macedonia
ditarm2@gmail.com

OPTIMIZATION OF STEEL FRAMES USING SEMI-RIGID CONNECTIONS

The true behavior of the connections is usually semi-rigid. Neglecting the real behavior of the connection in the analysis may lead to unrealistic predictions of the response and reliability of steel frames. In this paper the methodology for determination of rotational stiffness of semi-rigid connection in steel constructions according to Eurocode 3 componential method has been analyzed. By application of this concept the determination of rotational connection response comes down to determination of geometrical characteristic of different connection components. This paper considers the effects of semi-rigid behavior of the connections in analysis for steel frames and ways for global optimization of structural members and optimization of joint especially. In this paper, steel frames are analyzed by using computer program. Having the same geometry and cross-section, the static analysis for frames is examined for three different type of connections. The first frame is analyzed with ideally rigid connection, second one with semi-rigid connection and third one with ideally pinned connection.

Keywords: semi-rigid, joint, moment resistance, steel frame, rotational stiffness

1. INTRODUCTION

A steel frame as a plane of linear members, such as beams and columns, joined together by connections. These joints between members play an important role. From an economic point of view the costs for design and fabrication form a considerable part of the total cost. From a structural point of view the properties of the joint essentially influence the response of the structure to actions. Traditionally, in the design and analysis of steel frames it is assumed that all structural beam-to-column connection behave either as: simply pinned or fully rigid.

Simply pinned, which implies that no moment will be transmitted between the beam and the column and thus the connection is only capable of transmitting shear and axial force. As far as rotation is concerned, the beam and the column that are jointed together by a pin will behave independently.

Fully rigid, which implies that no relative rotation will occur between the adjoining members and the beam end-moment is transmitted to the

column. The angle between the beam and the column remains unchanged as the frame deforms.

Existing methods of design and analysis of steel frames still firmly rely on these simplified idealized models, despite the fact that it has been recognized for more than half a century that connection behavior lies somewhere between the two extreme idealizations. Thus the design of the structure is not fully based on the actual load-deformation characteristic of the joint. This is due to a member of factors, two of which are the relative complexity of the necessary design calculations and lack of comprehensive information on the performance of the full range of modern days connections. This has resulted in a rapid growth of investigation on this topic, leading to continuous innovations in the analysis and design of steel frames and the testing of beam-to-column connections. Experiments carried out during the last decades have shown that the behavior of real bolted connection is neither rigid nor pinned; rather, they possess some degree of rotational restraint which depend on type of connection used. The term "Semi-rigid" is used to describe such connections. In addition to the classification by rigidity beam-to-column connection may be classified as well by strength with respect to the design moment resistance. Under such classification beam-to-column connection behave wither as: nominally pinned, full-strength; partial-strength connection.

2. GENERAL DESCRIPTION OF ANALYTICAL MODEL

In this paper is analyzed a single span steel frame with dimensions 6.00x4.00m (L x H). Two columns are with cross-section HEA 180, beam with cross-section IPE 270. Base support for columns are ideally rigid connecting with concrete foundation. For this study connection beam-column is taken in three ways: ideally rigid, semi-rigid, ideally pinned. Frame is analyzed by two type of load. First load, include self-weight and uniform linear load 8.00kN/m'. Second load include vertical support displacement in column support for 5.0cm. Base support displacement is taken into account because this load can best determinate the behavior of frames in dependence of real connection rotation. In real situation non uniform foundation displacement shows in a lot of forms. For example, when we have to build very close to another building. In this situation

in that older building is done soil consolidation, that's mean a foundation for new building who is close to that have to do less consolidation in comparison on another foundation in same new building (in another column).

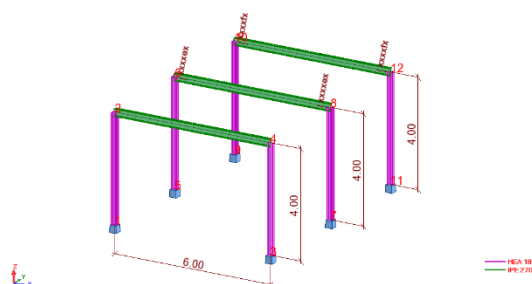


Figure 1. Steel frame, dimensions, cross-sections

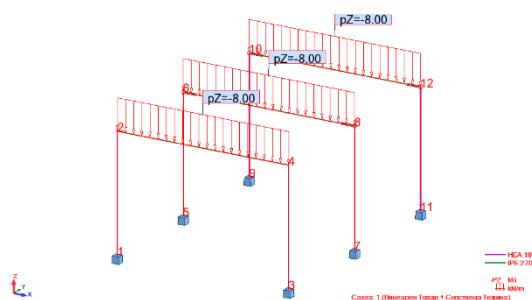


Figure 2. First load, self-weight and uniform linear load

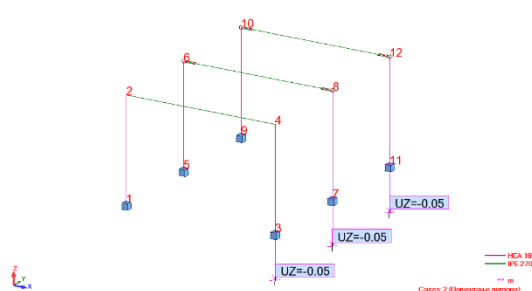


Figure 3. Second load, base support displacement

3. RESPONSE OF JOINT AND DESIGN TOOLS

Beside the need for background information the engineer requires simple design tools to be able to design joint in an efficient way. Three different types of design aids can be provided: -design tables; -design sheet; -software. Response of the joints in terms of stiffness, resistance and ductility is a key aspect for design purposes. From this point of view, three main approaches may be followed:

- experimental;
- numerical;
- analytical

In this paper is used the analytical approach. Analytical procedures enable a prediction of the joint response based on the knowledge of

the mechanical and geometrical properties of the so-called “joint components”. Component method applies to any type of steel joint whatever the geometrical configuration, the type of loading (axial force and/or bending moment, ...) and the type of member cross sections.

However, the analysis of a frame with semi-rigid connections is difficult to perform unless the exact moment-rotation relation of such joint is known.

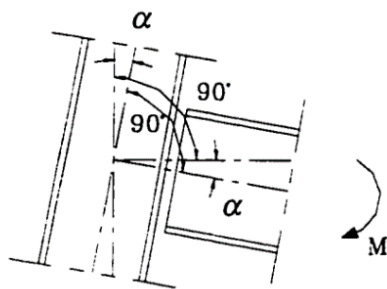


Figure 4. Loaded rigid connection

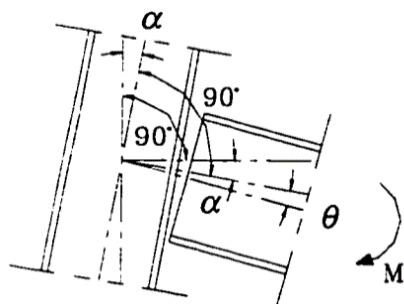


Figure 5. Loaded semi-rigid connection

At rigid connection moment-rotation relation is known before starting design of joint, at loaded rigid connection relative rotation between elements in elastic area is always 90°. Relative rotation between elements in elastic area at semi-rigid connection is shown with moment - rotation curve.

$$\theta_r = \frac{M}{S_{j,ini,s}} \quad (1)$$

where:

- θ_r : relative rotation between elements
- M: bending moment
- $S_{j,ini,s}$: Initial stiffness

3.1 DESIGN OF JOINTS ACCORDING EC3

Identification of the active components in the joint are regulated in EC3 part .1-8 (table 6.10). In this joint in figure 5, active components are:

1. Column web panel in shear; 2. Column web in compression; 3. Column web in tension; 4. Column flange in bending; 5. End-plate in bending; 10. Bolts in tension. For this connection in analytical way is calculated bending resistance, secant and initial stiffness.

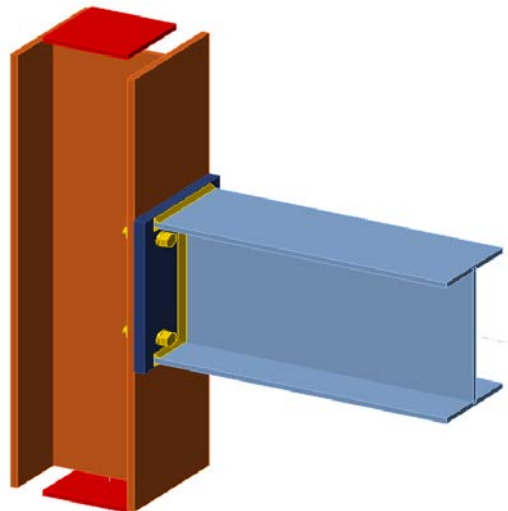


Figure 6. Single-sided bolted end plate connection used in this paper

Identification of the active components in the joint are regulated in EC3 part .1-8 (table 6.10). In this joint in figure 5, active components are:

1. Column web panel in shear; 2. Column web in compression; 3. Column web in tension; 4. Column flange in bending; 5. End-plate in bending; 10. Bolts in tension. For this connection in analytical way is calculated bending resistance, secant and initial stiffness.

Table 1. Joint components

Component	Stiffness coefficient k_i (mm)	Design Resistance $\min F_{Rd,i}$ (kN)
1. Column web panel in shear	2.374	177.30
2. Column web in compression	5.700	181.85
3. Column web in tension	6.540	199.6
4. Column flange in bending	3.419	115.13
5. End-plate in bending	11.320	180.86
10. Bolts in tension. 4M16	4.567	180.86

3.1.1 Design moment resistance:

$$M_{j,Rd} = F_{Rd} * z = 27.05 \text{ kN/m}' \quad (2)$$

3.1.2 Design elastic moment resistance:

$$M_{j,el,Rd} = \frac{2}{3} F_{j,Rd} = 18.03kN/m' \tag{3}$$

3.1.3 Initial stiffness:

$$S_{j,ini,s} = \frac{Eh^2}{\sum k_i} = 8614.12kNm/rad \tag{4}$$

3.1.4 Secant stiffness:

$$S_j = \frac{S_{j,ini,s}}{2} = 4307kNm/rad \tag{4}$$

3.1.5 EC3 classification of connections by stiffness:

$$k = \frac{S_{j,ini}L_b}{EI_n} = 4.250 \tag{5}$$

4. DESIGN OPPORTUNITIES FOR OPTIMISATION OF FRAMES

The various approaches can be used to design steel frames with due attention being paid to the behave of the joints. For the design of steel frames, the designer can follow one of the following design approaches: 1. Traditional design approach; 2. Consistent design approach; 3. Intermediate design approach.

In this paper is used consistent design approach, the global analysis is carried out in full consistency with the presumed real joint response. Both members of steel frame and joint properties are accounted for when starting the global frame analysis.

In the pre-design phase, joints are selected by the practitioner based on his experience. Proportions for the joint components are determined: end-plate or cleat dimensions, location of bolts, number and diameter of bolts, sizes of column and beam flanges, thickness and depth of column web, etc. First the joints are characterized with the possible consequence of having a non-linear behave. This characterization is followed by an idealization, for instance according to a linear or bi-linear joint response curve, which becomes a part of the input for global frame analysis. For the purpose of global frame analysis, any joint structural response is assigned to a relevant spring in the frame model.

5. NUMERICAL MODEL AND RESULTS

In this case study, the numerical analysis of steel frame is made with Autodesk Robot

Structural Analysis Professional). Globally speaking, four main analysis approaches may be contemplated according to Eurocode 3:

- linear elastic first order analysis;
- plastic first order analysis;
- linear elastic second order analysis;
- plastic second order analysis;

In this case study analysis is made with: linear elastic first order. Results for bending moments are shown in Combination of first load type together with second load type.

5.1 BENDING MOMENTS

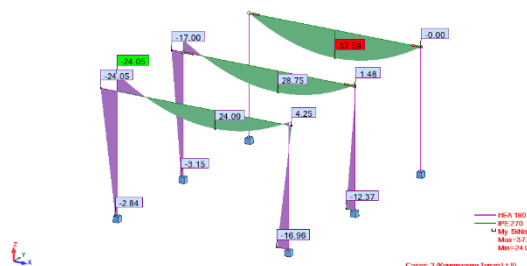


Figure 7. Bending moment on steel frame

Table 2. Bending moments

	Bending moments "My" from combination I+II (kN/m')		
	Negative moment "left joint"	Positive moment in middle of beam	Negative moment "right" joint"
Frame with rigid connection	-24.05	23.44	-4.25
Frame with semi-rigid connection	-17.00	28.75	-1.48
Frame with pinned connection	0.00	37.59	0.00

From the results at table 2. we can see that the maximum negative moment is at frame with rigid connection and maximum positive moment is at frame with pinned connection.

Joint designed in chapter 3 has elastic moment resistance 18.03kN/m'. From the table we can see that frame with rigid connection has negative moment value more than elastic moment resistance of joint. Also frame with pinned connection has higher positive bending moment than frame with semi-rigid and rigid connection.

5.2 DISPLACEMENTS

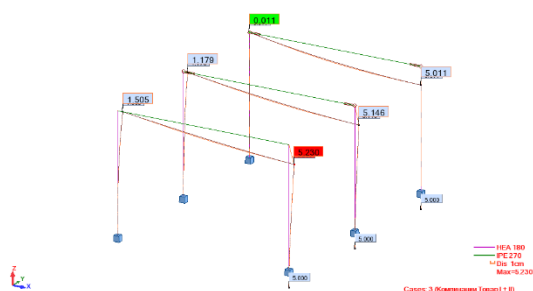


Figure 8. Deformation on steel frame

Table 3. Displacements

Frame	No de	Case	UX (cm)	UZ (cm)
Steel frame with "rigid" connection	1	3 (C)	0.000	0.000
	2	3 (C)	1.505	-0.012
	3	3 (C)	0.000	-5.000
	4	3 (C)	1.501	-5.009
Steel frame with "semi-rigid" connection	5	3 (C)	0.000	0.000
	6	3 (C)	1.179	-0.012
	7	3 (C)	0.000	-5.000
	8	3 (C)	1.177	-5.010
Steel frame with "pinned" connection	9	3 (C)	0.000	0.000
	10	3 (C)	0.000	-0.011
	11	3 (C)	0.000	-5.000
	12	3 (C)	0.000	-5.011

From the results at table 3. We can see that maximum node displacement (nodes where are connecting beam-column) has frame with rigid connection.

5.3 RELATIVE ROTATION BETWEEN MEMBERS

Table 4. Relative rotation between members

Frame	No de	Bending Moment (kN/m')	Initial stiffness (kNm/rad)	θ_r (rad)
Steel frame with "semi-rigid" connection	6	-17.000	8614.12	-0.00197
	8	-1.480	8614.12	-0.0001718

At rigid connection relative rotation between elements in elastic area is always 90°. At pinned connection there are no developing significant moments which might adversely affect members of the frame.

6. CONCLUSION

Based on the numerical results the following can be concluded:

1. In general designers when have to design a frame with support displacement goes with pinned connection, due the fact frame can rotate and not showing extra bending moments and lateral displacement. In this case frame with pinned connection have higher positive bending moments, which brings larger cross-section of beam.
2. Frame with rigid connection are more usually used in steel industries. From the table we can see that frame with rigid connection has negative moment value more than elastic moment resistance of joint (18.03kN/m'), which brings design a new joint detailing, more complex, more stiffener that brings increasing fabrication cost.
3. From the table we can see frames with rigid connection have higher lateral displacement, the higher lateral displacement can bring in more complex analysis (second order analysis)
4. Using semi-rigid connection shows a real optimization of steel frames. From the tables we can see, lower positive moments compare with pinned connection, and lower negative moments compare with rigid connection. Lateral displacement are lower compare with rigid connection.

5. A real advantage of using semi-rigid connection is taking relative rotation of members in joint for global displacements in frames. Which members can rotate and not showing extra bending moments.
6. Consistent design approach is more complex, need more time and work, but using this design we can bring more reliable results with taken care a real joint response. Consistent design approach brings optimization of joints components and cross-sections of members.

7. REFERENCES

- [1] EN 1993-1-1: Eurocode 3: Design of steel structures – Part 1-1: General rules and rules for buildings
- [2] EN 1993-1-8: Eurocode 3: Design of joints
- [3] Wai-Fah, Chen Norimitsu, Kishi Masato Komuro: “*Semi-rigid connections handbook*” (2011); ISBN: 978-1-932159-99-8
- [4] Jean-Pierre Jaspart Klaus Weynand; “Design of joints in steel and composite structures” (2016) ISBN (ECCS): 978-92-9147-132-
- [5] Zoubir Benterkia; “End-plate connections and analysis of semi-rigid steel frames” (PhD dissertation, 1991) University of Warwick
- [6] Mahmoud Hassan El-Boghdadi; “Elastic plastic analysis of semi-rigid industrial frames” (PhD dissertation, 1997)
- [7] Chen, W. F. (editor), *Practical analysis for semi-rigid frame design*, World Scientific, Singapore, 2000

Mihail Naumovski

BSc, Teaching Associate
University “Ss. Cyril and Methodius”
Faculty of Civil Engineering – Skopje
naumovski@gf.ukim.edu.mk

Marijana Lazarevska

PhD, Associate Professor
University “Ss. Cyril and Methodius”
Faculty of Civil Engineering – Skopje
marijana@gf.ukim.edu.mk

Darko Dimkovski

MSc, Building Engineer
Rapid Bild doo Kumanovo
Str. Nikola Tesla No. 160, Kumanovo
darko.dimkovski@kvp.com.mk

COMFORT, AS AN ASPECT OF LIFE CYCLE ASSESSMENT (LCA) ANALYSIS TOWARD SUSTAINABLE BUILDINGS

Life Cycle Assessment (LCA) is a standardized, science-based methodology that has been developed to evaluate the environmental impact of buildings, with respect to their processes, their materials and use (energy) throughout the whole life cycle of a building. LCA takes into consideration all the steps that lead from raw material through manufacture, distribution and usage to final disposal. LCA in construction tends to evaluate the environmental impacts throughout the entire life cycle of the building, including upstream and downstream processes associated with the production and disposal. LCA is one of the most promising techniques for an ecological design of buildings. However, in order to appeal to the benefits of LCA, it is important to know how to use LCA properly.

In this paper, the use of LCA in the construction sector has been critically analyzed. The main aspects of LCA have been applied for a case study of a building in Copenhagen, Denmark.

Keywords: LCA analysis, comfort, LCA design, sustainable building, health life-being

1. INTRODUCTION

LCA is a branch of modern Building Engineering, defined as a method that is being increasingly used to evaluate the potential environmental impacts of products and services and their usages. Nowadays, LCA is also being used in building sector, especially where it is a crucial part of assessing buildings environmental sustainability. The life cycle approach focuses on factors related to the completed building to involve the entire life cycle of the building. Life Cycle Assessment (LCA) is included in European standards for sustainable construction, Construction Products Regulation (CPR) and the certification schemes for sustainable buildings at all. An important fact is that Life Cycle Assessment (LCA) is also named as an essential part of the focus area sustainable building in the Danish government's building policy strategy from 2014, which is partly why we have chosen such a current location of our sustainable building, i.e. a location in Copenhagen, Denmark

Life Cycle Assessment (LCA) provides a basic knowledge of the parameters that contribute to resource use and the potential environmental impacts during a building's life cycle for the different players working in assessing the environmentally related part of sustainable building. Incorporating LCA as a tool in the building design stage makes it possible to evaluate the environmental significance of building elements or the different life cycle stages of the building. LCA can thus be used as part of the environmentally friendly design of buildings and in documenting the results.

Life Cycle Assessment (LCA) can also point out the most important aspects of the sustainable development of building sector at all. It is clearly known that the modern Building Engineering aspires to aspects such as comfort of life – living. An aspect which contains everything that can affect on a psychological state of humans who use the building which is a subject of interest. Such an aspect can just offer more sustainable solutions to be achieved by shifting the focus from optimizing the building parts and products' lifetime, to considering their life cycles, either as whole components or as part of the production of new products.




1.1 A BUILDING'S LIFE CYCLE


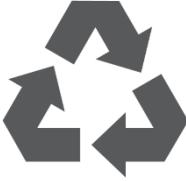
A life cycle assessment of a building involves typically evaluating its whole life cycle [1]. This means including all stages in the assessment such as: raw material supply, manufacture of construction products, the construction process stage, use stage, demolition, and when the materials are disposed of or recycled.

Therefore, the building's life cycle is divided into five stages that need to be dealt with: The product stage, construction process stage, use stage, the end-of-life stage, and benefits and loads beyond the system boundary.

The first two stages are often the best known, even though acquiring sufficient data for the calculations can be problematic in practice. The following three stages are scenario-based, which means that assumptions have to be made about how the building will be used, maintained, and finally demolished. According to European standard EN 15978:2011, the final stage of building waste recycling must be reported as a separate part of the calculations. These stages offer a quality life cycle towards a sustainable development. The five stages are described as follow:

Table 1. Stages of Building's Life Cycle [1].

1. STAGE: PRODUCT STAGE	
	<p>The product stage concerns the processes which involve the production of construction products used in the building: Raw material supply, transport to the production site as well as the final production of the construction products.</p>
2. STAGE: CONSTRUCTION PROCESS STAGE	
	<p>The construction process stage involves the construction products' journey from production line to the point where they are installed as a part of the finished building: Transport from the manufacturer to the construction site as well as installation in the building.</p>
3. STAGE: USE STAGE	
	<p>The use stage involves the processes related to the construction products' continued performance as part of the building, e.g. maintenance, replacement, repair. Processes related to the building's ongoing operational energy and water use are also included. Most often, the processes will be based upon scenarios, i.e. perceptions about how the processes will take place.</p>

4. STAGE: END OF LIFE STAGE	
	<p>The processes in this stage are also scenario-based. They concern what happens when the building reaches the end of its life, i.e. the building's demolition and the subsequent processes involved in reprocessing or handling the construction products/materials before further use of in other product systems.</p>
5. STAGE: BENEFITS AND LOADS BEYOND THE SYSTEM BOUNDARY	
	<p>This scenario-based stage contains the calculated gains and drawbacks from reusing and recycling construction products/materials. In accordance with the European standards, contributions from this stage must be considered outside the system boundary and be reported separately.</p>

1.2 WHAT DOES A BUILDING'S LIFE CYCLE LOOK LIKE?

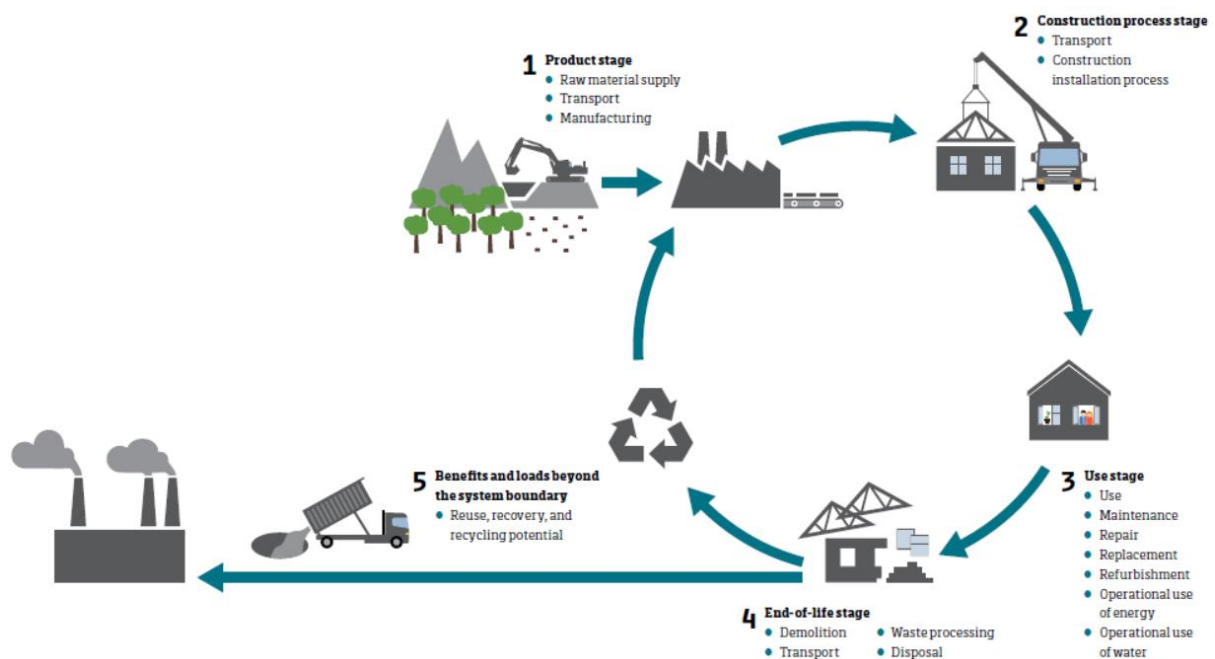


Figure 1. Typical stages of Building's Life Cycle [1].

Figure 1. illustrates the typical life cycle for a building and which stages and processes are involved (Typical stages of a building's life cycle: the product stage, the construction process stage, the use stage, the end of life stage and benefits and loads beyond the system boundary).

An Life Cycle Assessment (LCA) adds up all of the interactions with the environment which take place during the course of the included life cycle stages. The interactions may be in the form of for example, transport emissions or

resource consumption from the cultivation of trees.

1.3 A BUILDING'S LIFE CYCLE

Life Cycle Assessment (LCA) involves surveying all of the inputs and outputs linked to the examined system's life cycle. The potential environmental impacts are calculated based on all inputs and outputs, i.e., consumption of resources and emissions associated with the different processes.

1. Global Warming Potential (GWP) – Unit: CO₂ equivalents – Problem: When the concentration of greenhouse gasses in the atmosphere increases, the atmospheric layers near the earth are heated up, resulting in climate change.

2. Depletion Potential of the Stratospheric Ozone Layer (ODP) – Unit: R11 equivalents – Problem: Depleting the stratospheric ozone layer that protects flora and fauna against the sun's harmful UV-A and UV-B radiation.

3. Formation Potential of Tropospheric Ozone Photochemical Oxidants (POCP) – Unit: Ethylene equivalents – Problem: Contributes to UV radiation to ozone formation in the lower atmosphere (summer smog) is damaging to the respiratory system.

4. Acidification Potential (AP) – Unit SO₂ equivalents – Problem: When acidifying substances react with water and fall as 'acid rain, this leads to, among other things, decomposition of root systems and leaching of nutrients from plants.

5. Eutrophication Potential (EP) – Unit: PO₄ equivalents – Problem: An excessive supply of nutrients generated unwanted plant growth in delicate ecosystems, for example, the development of algae which results in the death of fish.

6. Abiotic Depletion Potential for non-fossil Resources (ADPe) – Unit: Sb equivalents – Problem: A high use of abiotic resources can contribute to the depletion of available elements, e.g., depletion of metals and minerals.

7. Abiotic Depletion Potential for Fossil Resources (ADPf) – Unit: MJ – Problem: Heavy consumption of abiotic resources can reduce available fossil energy sources such as oil or coal.

8. Total Use of Primary Energy (PE_{tot}) – Unit: MJ or kWh – Problem: A high use of resources in the primary energy form from fossil and renewable sources can contribute to the depletion of natural resources.

9. Use of Renewable Secondary Fuels (Sec) – Unit: MJ or kWh – Problem: Secondary fuels (e.g., waste) are in principle limited resources, and therefore a high use of secondary fuels can indirectly lead to scarcity of resources.

The aim of the project is to develop Life Cycle Assessment (LCA) of the case study in order to

define the impact of sustainability of the designed building. This goal is obtained following different steps as suggested by the reference codes and the steps are summed up in the following scheme:

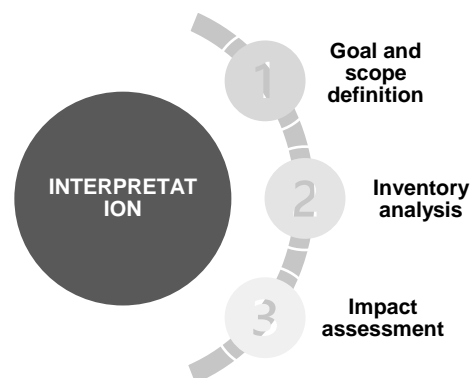


Figure 2. Scheme of Building's Life Cycle for defining the impact of sustainability.

Different assumptions will be shown before calculating the quantities of each material in order to assess the emissions of each single component of the functional unit. The results obtained in terms of production can be used in the Active House Protocol in order to fulfil the third category, which is the "ENVIRONMENT" category, and is composed of data for "Environmental loads", "Freshwater consumption" and "Sustainable construction" of the previously mentioned protocol.

2. GOAL AND SCOPE DEFINITION

Life Cycle Assessment (LCA) is a branch of modern Building Engineering. The most important step according to the codes is to define a goal and scope of the analysis in the Life Cycle Assessment (LCA) framework [2]. It is essential to determine what will be analyzed and why this content will be processed in the Life Cycle Assessment (LCA). The object of the study can be seen through different scenarios, and mainly two of them are considered in this project:

- Cradle to grave: from raw materials to the end of life of the building.
- Cradle to gate: from raw materials to the moment they reach the site and are installed.

This step aims to define the functional unit by answering five main questions of the case study (the residential building):

What? How Much? How long?
Where? How well?

In this case study, the functional unit had the purpose of permanent housing for a family of three members, providing proper comfort (in terms of daylight and energy) in 175 [m²] during the entirety of a year. The case study is located in Brønshøj, a municipality in Copenhagen, Denmark, with an intended life cycle of 50 years. The house is designed as a wooden structure with CLT technology. It has two bedrooms, a bathroom, a living room with a kitchen, a technical room, and two porches located on the ground floor, and on the second level, which is the mezzanine, it has a small library, bedroom, and a small bedroom toilet. The house has a spectacular view, overlooking the river from its south side. Refer to the functional unit, it is crucial to define the reference flow. According to the Active House Protocol, the reference flow is generally the unit of the area [m²].

3. DESIGN OF THE BUILDING

3.1 ARCHITECTURAL DESIGN

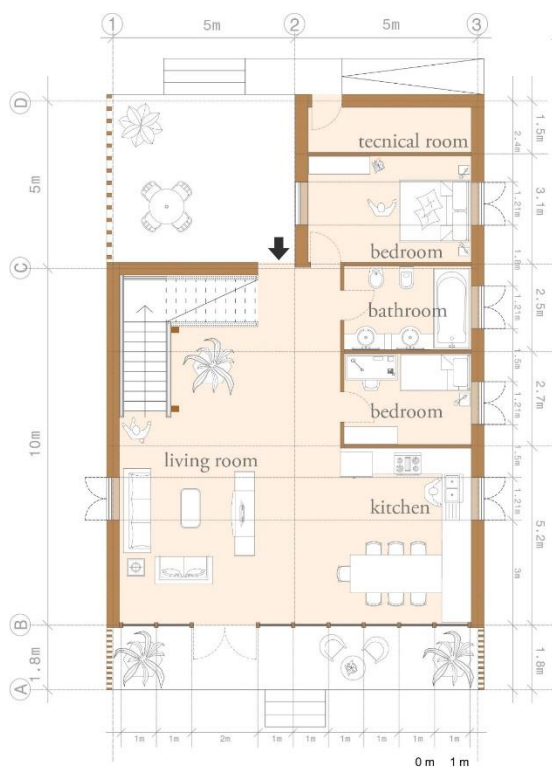


Figure 3. Architectural plan of ground floor.

As can be seen from the Figure 3., there are two entrances, the main entrance from the

porch facing North and the South door facing the river. The central part of the ground floor is the opened living room area with the kitchen composing a total of 90 [m²], one master bedroom with 18 [m²], one smaller bedroom for the child with 12 [m²], one main bathroom with 10 [m²], which altogether are defining the usable space for the ground floor, which is 130 [m²]. The south porch has 20 [m²], and the north porch has 25 [m²].

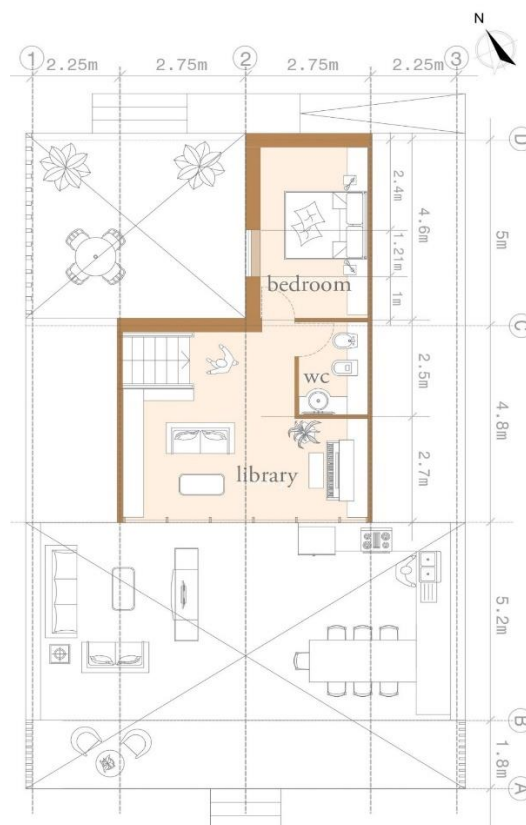


Figure 4. Architectural plan of mezzanine floor.

As it can be seen from the Figure 4., we have the living room staircase leading up to the opened library with a total area of 28 [m²], one small toilet with 4.5 [m²], and a guest bedroom with 12.5 [m²]. Altogether, they compose a total usable area of 45 [m²]. The ground floor and the mezzanine level together comprise an entire functional space of 175 [m²].

3.2 STRUCTURAL DESIGN

For what concerns the structural design, the structure itself is composed of the main ridge beam (30x50cm), seven primary beams (25x40cm), fourteen secondary beams (10x20cm), and external CLT walls amounting to 160.3 [m²].



Figure 5. Structural Design of the building.

3.3 DESIGN STRATEGIES

There are ten design strategies used:

1. The compact shape of the building decreases heat losses during winter.
2. The porch facing west is used to extend the living area protected from the wind (mainly blowing from west) and from the afternoon sun.
3. Two solar panels facing east are used to heat water for the occupants.
4. Transparent surfaces are mostly facing south to maximize solar gains in winter (maximum sun height is 11 degrees).
5. A shaded porch facing south is used to limit glare and solar gains in summer (maximum sun height is 58 degrees).
6. Transparent surfaces are arranged in such a way to have the best connection with the outdoor and view of the landscape.
7. Transparent surfaces are added to the roof to exploit natural light and ensure better indoor daylight.
8. Openable skylight assures ventilation through stack effect for the exchange of air.
9. Windows are placed on all four sides of the house to exploit cross ventilation.
10. Twenty photovoltaic panels facing east are used to cover 30% of the electricity demand of the building.

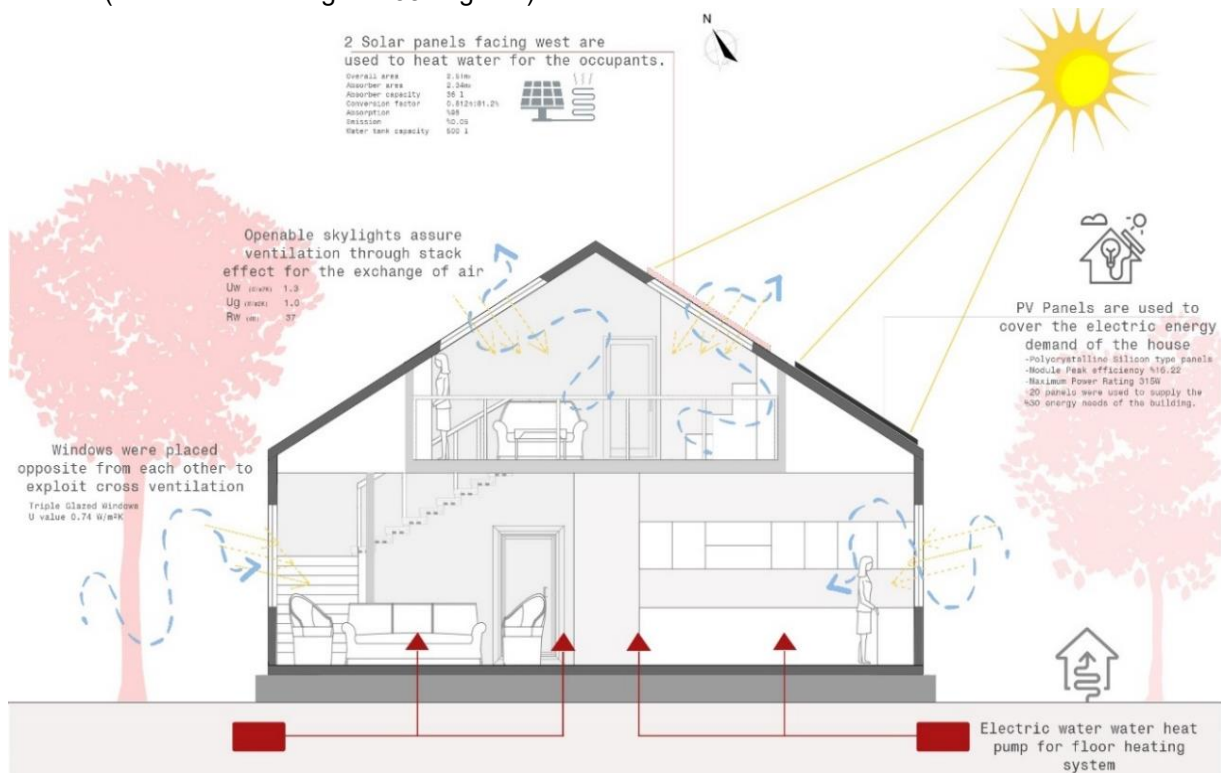


Figure 6. Design strategies applied on the building.



Figure 7. South view of the residential unit (south porch and big curtain wall overlooking the river) towards climatic design.



Figure 8. West view of the residential unit (south porch and big curtain wall overlooking the river) towards climatic design.

3.4 CLIMATIC DESIGN

Temperature: Dry bulb's external temperature ranges between 12°C and 23°C most of the hours. The coldest months are February and December, in which temperatures go below zero, while the hottest month is August, in which it is reached a temperature greater than 27°C.

Sunpath: At West, during the afternoon, external outdoor dry bulb temperature is higher, so there is the need to bring building surfaces away from the western sun. It is better to face most of the glass area to the South for passive solar heating to maximize winter sun exposure, but design overhands to fully shade in summer. The maximum declination angle of the sun is 58° (21st July), and the minimum is 11° (21st December).

Radiation: Radiation is mainly coming from the South. A North diffused radiation has to be exploited. Any passive solar gain is a benefit since the danger of overheating is minimal.

The wind rose: Wind blows mainly from the West and has a moderate velocity. Sunny wind-protected outdoor spaces can extend living areas in cool weather like in Copenhagen.

4. METHODOLOGY

For this project, much software has been used to realize the Life Cycle Assessment (LCA) evaluation [3], [4], [5], [6], [7], [8]. Since the Life Cycle Assessment (LCA) evaluation consists of 3 main categories, each of 3 subcategories, much data needs to be analyzed to achieve a reliable result.

The aspect that is dedicated to Comfort and is subdivided into Daylight, Thermal Environment, and Indoor Air Quality.

For what concerns Daylight, a VELUX daylight visualizer has been used to obtain the required parameters. Three main parameters can be extracted from the software, and they are the Daylight factor (percentage of indoor to outdoor illuminance under CIE overcast sky conditions), the Illuminance (the amount of light that reaches a surface), and Illuminance (the amount of light reflected off a cover).

Dynamic simulations have been done in the software IES-VE (Integrated Environmental solutions) for the Thermal Environment and Indoor Air Quality.

5. WHAT ARE THE RESULTS? – COMFORT AND ITS SUBDIVIDES

The comfort analysis in the Active House specification [10] promotes solutions for people to live in comfortable buildings in terms of daylight, thermal comfort, and indoor air quality, which is mainly needed because people living in modern societies spend 90% of their time indoors.

For comfort purposes, the shape and orientations of an Active House are optimized to the external climate: in fact, the house is oriented with the big curtain wall placed at South and big skylights to gain the highest amount of solar radiation possible. Furthermore, the West porch has been designed to create an outdoor living area protected from the wind that flows at a speed greater than 19 m/s.

The envelope has been designed with high thermal insulation thickness to insulate the building well since the temperatures are rigid during winter, while openings have been placed in the proper position to exploit cross-natural ventilation and stack effect during the summer months.

5.1 DAYLIGHT

The building has been designed to have natural daylight as the primary light source to reduce the electricity needs for artificial lighting.

High daylight values reached through large transparent surfaces are essential to be achieved (also to guarantee the requirement of being in contact with nature and thus the well-being of the occupants).

The parameter "Daylight Factor" shown in Table 2. has been assessed through the Velux software to evaluate the house's daylight condition: it is defined as the illuminance on a surface expressed as a percentage of the external diffused illuminance.

Table 2. Classes towards "Daylight factor".

CLASS	DAYLIGHT FACTOR
1	DF > 5% on average
2	DF > 3% on average
3	DF > 2% on average
4	DF > 1% on average

Before calculating the daylight factor in our house with all the strategies selected, we also wanted to show how much do our choices affect this parameter: so first of all, we calculated the daylight factor considering the absence of fixed shading systems (placed at South and West), and then we made a comparison with the results obtained with the fixed shading systems applied. Results show that the shading devices perform well, especially

in summer, in the living room when the risk of glare is high, but during winter, the level of light is not sufficient in all the houses, this also happens in the rooms with no shading devices applied, and the reason is that the solar radiation is not much at the latitude of Copenhagen.

The daylight factor is assessed room by room: each factor is weighted to give an average daylight factor for each room. The calculation should also consider neighboring buildings, but no other buildings create shades in the site studied. The evaluation includes the living and activity zones (such as living room, workspace, dining room, kitchen, bedroom, or children's room). The room with the lowest daylight factor score sets the overall daylight factor for the building.

Looking at the results, for what the ground floor concerns, it is visible that the living room with the kitchen has the highest average daylight factor due to the presence of the curtain wall (it is essential to underline that only the fixed shading system has been considered, so the need of movable internal curtains is necessary to avoid the risk of glare). The other rooms (bedrooms) have lower daylight since they are exposed only to the East (apart from the master bedroom exposed to both East and West, but a porch shades the West side) and does not have skylights. Results are outstanding due to the strategic position of the skylights, considering the mezzanine: CLASS is between 1 and 2.

The Active House tool measures the class's greater precision, and after inserting the necessary data for every individual room, the output result says that Class 1.4 is reached.

AVERAGE VALUES - DAYLIGHT FACTOR - Ground floor		AREA [m ²]	CLASS
Living room – front part overlooking the south	1.80 [%]	35 [m ²]	1
Living room – the part facing the main entrance	10.80 [%]	55 [m ²]	
Bedroom for children	2.00 [%]	12 [m ²]	3
Bathroom	2.20 [%]	10 [m ²]	3
Master bedroom	2.60 [%]	18 [m ²]	3
DAYLIGHT FACTOR (AREA WEIGHTED)	5.73 [%]	130 [m²]	/
AVERAGE VALUES - DAYLIGHT FACTOR - Mezzanine floor		AREA [m ²]	CLASS
Mezzanine area	4.90 [%]	28 [m ²]	2
Bathroom	7.30 [%]	4.50 [m ²]	1
Bedroom	6.00 [%]	12.5 [m ²]	1
DAYLIGHT FACTOR (AREA WEIGHTED)	5.45 [%]	45 [m²]	/

CONCLUDED RESULT:

DAYLIGHT FACTOR - (AREA-WEIGHTED)	5.68 [%]	175 [m²]	1
--	-----------------	----------------------------	----------

1.1 Daylight		
Daylight factor		
Room type	Project	Reference
Living room 1	6.3	0
Bedroom 1	2	0
Bathroom 1	2.2	0
Bedroom 2	2.6	0
Living room 2	4.9	0
Bedroom 3	6	0
Bathroom 2	7.3	0

Daylight score:		
	Project	Reference
Validated simulation program:	yes	yes
Daylight factor score:	1.4	Out of AH category

Figure 9. Output of Software Daylight Class.

5.2 THERMAL ENVIRONMENT

A thermal environment is vital for comfort in buildings: different local temperatures of the air inside the other areas of the house can cause thermal discomfort, and for this reason, the envelope should be designed well.

The Active House Specifications use the adaptive approach to evaluate the thermal environment. The idea behind the method is that people adapt to the outdoor temperature as it rises and falls. We adapt psychologically by adjusting our activity, clothing level, or opening or closing windows. The adaptive method uses the outdoor running mean temperature (T_m) to vary the comfort limits. Requirements should be met for at least 95% of the hours.

Table 3. Classes towards temperature.

CLASS	HEATING SEASON	COOLING SEASON
1	$T_{i,o} > 21^{\circ}\text{C}$	$T_{i,o} < 25.5^{\circ}\text{C}$
2	$T_{i,o} > 20^{\circ}\text{C}$	$T_{i,o} < 26^{\circ}\text{C}$
3	$T_{i,o} > 19^{\circ}\text{C}$	$T_{i,o} < 27^{\circ}\text{C}$
4	$T_{i,o} > 18^{\circ}\text{C}$	$T_{i,o} < 28^{\circ}\text{C}$

In the building, calculations have been dynamically performed (in summer and winter), considering first the absence of heating or cooling systems, then with systems on to show how much the envelope can affect the indoor temperature.

From the chart, at Figure 10., it is visible that the envelope, without the use of the systems, performs well only with the help of passive strategies. Indoor operative temperatures increase by 8°C concerning the outdoor temperature in winter, and in summer, the indoor operative temperature increases by only 2°C . Heating hours decreased even if there is still a high need for heating while cooling hours increased in the central months of the year. Thanks to the good performances of the envelope, the building will have lower energy demand, and then cooling and heating systems will require low energy consumption, and the plants will have reduced dimensions. Considering the use of heating and cooling systems results obtained are the following, that are shown in Figure 11.

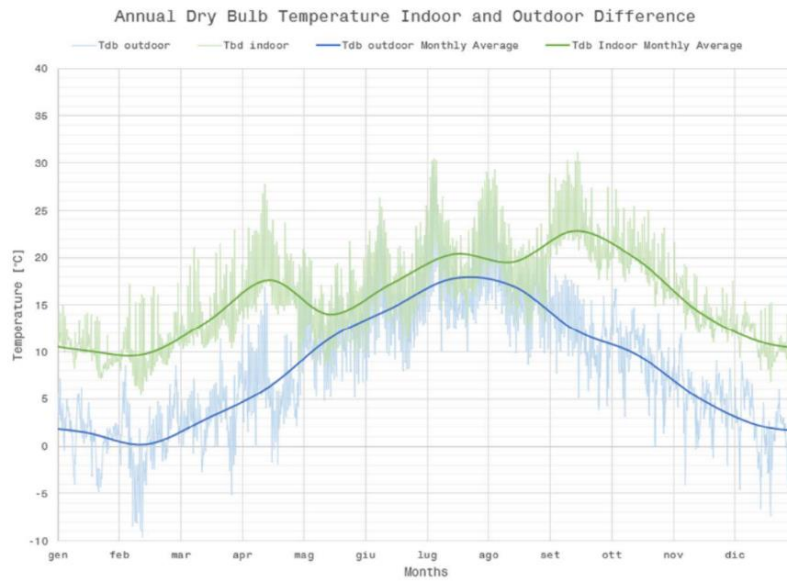


Figure 10. Indoor and Outdoor Temperature Distribution.

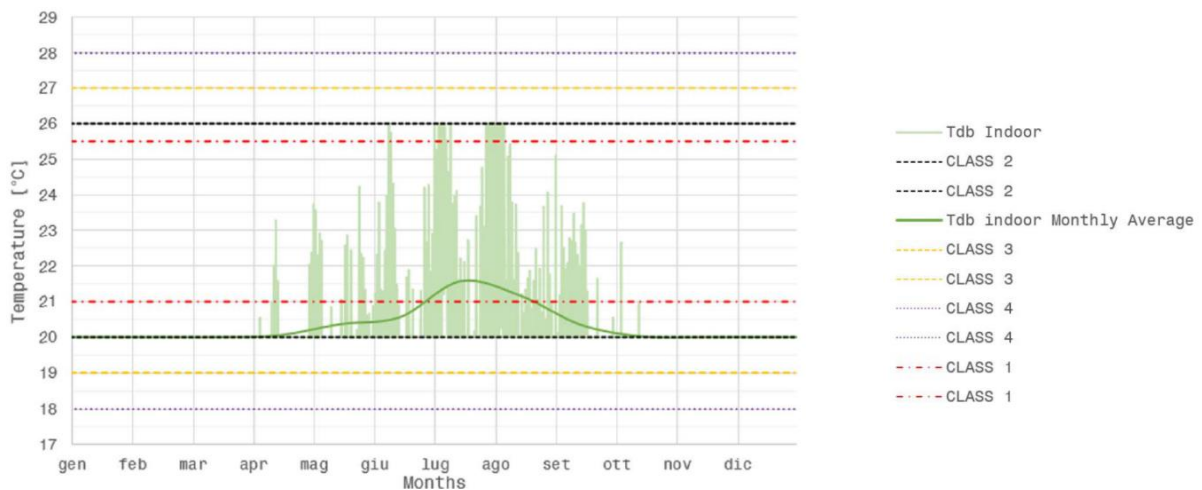


Figure 11. Indoor Temperature Distribution with the use of the HVAC system.

Indoor operative temperature and classes ranges have been plotted hourly in the chart. With a set-point for heating equal to 20°C and a set point for cooling equal to 26°C indoor operative temperature stays between the limits of CLASS 2. It coincides with the lower limit

during the whole heating season, while the upper limit is reached only for a short period between July and August. All the necessary data has been inserted into the Active House Tool, and the following results are obtained:

MINIMUM TEMPERATURE (winter)			OVERHEATING (summer)		
Category	Hours	Percentage	Category	Hours	Percentage
1	114	1.9%	1	2645	95%
2	5976	100%	2	2784	100%
3	5976	100%	3	2784	100%
4	5976	100%	4	2784	100%
Total	5976		Total	2784	

CONCLUDED RESULT:

THERMAL ENVIRONMENT	
MAXIMUM OPERATIVE TEMPERATURE	1
MINIMUM OPERATIVE TEMPERATURE	2

Thermal environment score		
	Project	Reference
Dynamic simulation:	yes	yes
Project stage:	Design (use of standards)	Planning (use of Active House Tool)
Thermal environment category:	Better level	Out of AH category
Thermal environment score:	1.5	Out of AH category

Figure 12. Output of Software Thermal Environment Class.

CLASS 2 is defined in the winter period because 100% of the time, indoor operative temperature is in this range. For the cooling period instead, CLASS 1 is defined because 95% of the time, the indoor operative temperature stays in the scope of the first class, while the remaining 5% falls in the range of the second class.

5.3 AIR QUALITY

The goal of an Active House concerns good air quality inside the house while minimizing the energy used for ventilation: for this reason, natural ventilation should be exploited whenever possible.

Nowadays, people spend most of their time indoors, and good indoor air quality can prevent occupants from getting irritations, asthma, allergy, or even cardiovascular diseases. Also, odor problems are reduced, and this affects the overall well-being of the people inside.

The CO₂ indoor concentration has been classified as a good indicator of indoor pollutants generally related to human activities to evaluate the fresh air supply. For this reason, hourly CO₂ concentrations are determined with a dynamic simulations tool (IES-VE in the case studied), considering standard occupancy rates and the standard CO₂ production per person.

Values obtained are then compared with the outdoor levels of CO₂, and requirements should be met for a minimum of 95% of the occupied time.

Outdoor CO₂ concentration in Copenhagen ranges between 340 ppm and 450 ppm, depending on the hour of the day and the urbanization of the territory. Calculations of the limits according to the classes have been carried out considering both the lower and upper layers. The first chart considers the lower CO₂ concentration level, and the second one the higher concentration level.

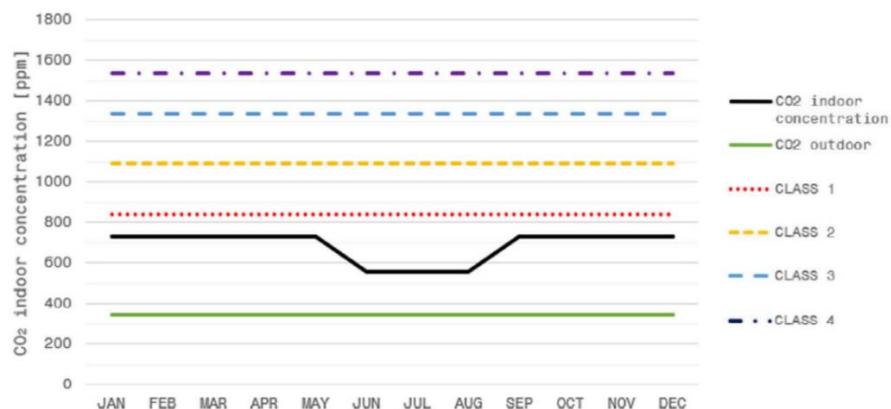


Figure 13. Indoor CO₂ concentration considering the lower limit.

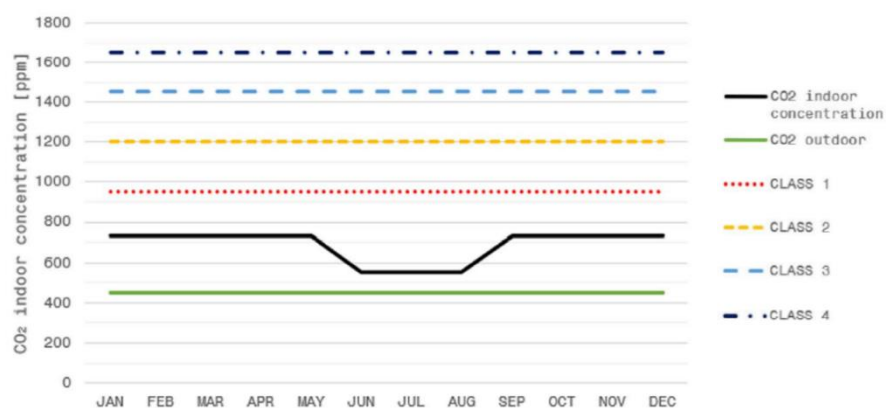


Figure 14. Indoor CO₂ concentration considering the upper limit.

The fresh air supply shall be established according to the limit values for indoor CO₂ concentration in the building occupied for a prolonged period with people as the dominant source. CO₂ concentration classes are calculated starting from the value of outdoor concentration

Table 4. Classes towards CO₂ concentration.

ACTIVE HOUSE PROTOCOL	
CLASS	CO ₂ concentration
1	< 500 ppm
2	< 750 ppm
3	< 1000 ppm
4	< 1200 ppm

Results show that CO₂ indoor concentration is 731 ppm during the winter period and 555 ppm during the summer period: this means that in both the situations (upper or lower limit of outdoor CO₂ concentration considered), the difference between indoor and outdoor levels is below 500 ppm and so CLASS 1 is reached for 100% of the hours. The correct exploit of natural ventilation during summer due to the windows' position cross ventilation and the skylights that enable the stack effect causes the reduction of the pollutants inside the ambient. All the necessary data has been inserted into the Active House Tool, and the following results are obtained:

CO ₂ concentration (winter)			CO ₂ concentration (summer)		
Category	Hours	Percentage	Category	Hours	Percentage
1	5976	100%	1	2784	100%
2	5976	100%	2	2784	100%
3	5976	100%	3	2784	100%
4	5976	100%	4	2784	100%
Total	5976		Total	2784	

CONCLUDED RESULT:

INDOOR AIR QUALITY	
STANDARD FRESH AIR SUPPLY (overall)	1
STANDARD FRESH AIR SUPPLY (summer)	1
STANDARD FRESH AIR SUPPLY (winter)	1

Air quality score		
	Project	Reference
Project stage:	Planning (use of Active House Tool)	Planning (use of Active House Tool)
CO ₂ -concentration above outdoor:	≤ 500 ppm	> 1200 ppm
Indoor air quality score:	1.0	Out of AH category

Figure 15. Output of Software Air Quality Class

In this case, the results given from the software confirm the results obtained manually, and so, during the whole year, CLASS 1 of CO₂ concentration is reached 100% of the time.

6. CONCLUSION

A functional residential unit has been designed by implementing the use of standards, resource guides, simulation software and Active House Design Specifications. Natural Daylight has been exploited by proper positioning of glazing surfaces, Good Thermal Environment has been created by the implemented design strategies and Indoor Air Quality is at a good level according to the Active House Specifications. Two types of simulation tools have been used in order to gain accurate results for the purpose of the Active House approach: VELUX daylight visualizer [12] has been used to the category of Daylight, and IES-VE (Dynamic Simulation Software) has been used for the categories Thermal Environment and Indoor Air Quality. After performing the analysis for the first main category (Comfort) according to the Active House Specifications we can say that the building performs really well in terms of “Comfort”: CLASS of 1.4 has been achieved for “Daylight”, CLASS of 1.5 for “Thermal Environment” and CLASS of 1.0 for “Indoor Air Quality”.

All in all, as a conclusion of the paper we could say that not even for luxury, but also more important for social health of humans, comfort must be treated as an aspect of Life Cycle Assessment (LCA) analysis of the buildings. Comfort undoubtedly offers a health a wide range of benefits which are at first good for the building humans live in, and after that for the general life – being of humans. We also find out that such a Life Cycle Assessment (LCA) analysis could be carried out many aspects touched but the materials which are used, the construction of the building, economical aspects and as we said the most important ones: social – health aspects. For now and further, especially building sector, must develop a different frame of thinking of the building. Not only the construction of the buildings should be discussed, but also from modern topics such a comfort, can make a better building in which everyone it used, can have better tomorrow.

REFERENCES

- [1] Birgisdottir H., Rasmussen N. F (2016), *Introductuin to LCA of Buildings*, 1st edition, Publisher: Danish Transport and Construction Agency Edvard Thomsens Vej 14, 2300 KobenhavnS, IBN 978-87-90661-59-5.
- [2] Danish Ministry of Environment, with the consultants: Wenzel H. – Institute for Product Development, Petersen C. – Econet, Hensen K. – The Finish Building Research Institute (2004), *The Product, Functional Unit and Reference Flows in LCA*.
- [3] BS EN 15978:2011 – Sustainability of construction works – Assessment of environmental performance of buildings – Calculation method.
- [4] BS EN 15978:2011 – Sustainability of construction works – Assessment of environmental performance of buildings – Calculation method.
- [5] EN 12464-1 – Light and lighting – Lighting of workplaces - Part 1: Indoor workplaces.
- [6] BS EN ISO 14040:2006 – Environmental management – Life cycle assessment – Principles and framework.
- [7] BS EN ISO 14044:2006+A1:2018 – Environmental management – Life cycle assessment - Requirements and guidelines.
- [8] SO 15469:2004(E), *Spatial Distribution of Daylight – CIE Standard General Sky*. CIE Central Bureau, Vienna.
- [9] *Active House Guidelines - Version 1* - www.activehouse.info.
- [10] *Active House - The Specifications for Residential Buildings - 2nd edition* - www.activehouse.info.
- [11] Andersen A.P., Karsten D., Foldbjerg P., Roy N. (2008), *Daylight, Energy and Indoor Climate Basic Book*, Publisher: VELUX A/S, 2nd edition.
- [12] *VELUX Modular Skylights – Product Brochure* – Velux Company Ltd – Woodside Way, Glenrothes, Fife KY7 3ND – www.velux.co.uk/domesticmodularskylights.
- [13] Assegio de L. R., Calleja G. Cejudo M. J., Raguei M., Faullana i Palmer P. (2014), *A decision-making LCA for energy refurbishment of buildings: Conditions of comfort*, Publisher: Energy and Buildings.
- [14] Santos P., Pereira A. Gervasio H., Mateus D., Bettencourt A. (2017), *Assessment of helath and comfort criteria in a life cycle social contex: Application to buildings for higher education*, Publisher: Building and Environment 123.



SELECT A PROFESSION

CREATIVE	SOPHISTICATED	RECOGNIZED	RESPONSIBLE
ENDURING	UP-TO-DATE	WORLWIDE	IMPORTANT

WWW.GF.UKIM.EDU.MK



OUR FACULTY CAN GIVE YOU

IMPULSE !	SCHOLARSHIPS FOR THE BEST	ASSURANCE !	COOPERATION WITH INDUSTRY AND INTERNATIONAL UNIVERSITIES
SIMPLE ENROLLMENT	MOTIVATION !	100% EMPLOYMENT AND INTERNATIONALLY RECOGNIZED DIPLOMA	SUPPORT !

WWW.GF.UKIM.EDU.MK

Ivona Nedevska

MSc, Teaching Assistant
University “Ss. Cyril and Methodius”
Faculty of Civil Engineering – Skopje
nedevska@gf.ukim.edu.mk

Zlatko Zafirovski

PhD, Assistant Professor
University “Ss. Cyril and Methodius”
Faculty of Civil Engineering – Skopje
zafirovski@gf.ukim.edu.mk

Marijana Lazarevska

PhD, Assistant Professor
University “Ss. Cyril and Methodius”
Faculty of Civil Engineering – Skopje
marijana@gf.ukim.edu.mk

Riste Ristov

MSc, Teaching Assistant
University “Ss. Cyril and Methodius”
Faculty of Civil Engineering – Skopje
ristov@gf.ukim.edu.mk

Vasko Gacevski

MSc, Teaching Assistant
Ss. Cyril and Methodius University
Faculty of Civil Engineering – Skopje
gacevski@gf.ukim.edu.mk

TRACK GEOMETRY DEGRADATION AND MAINTENANCE OF THE RAILWAYS

Today, rail networks across the world are getting busier with trains travelling at higher speeds and carrying more passengers and heavier axle loads than ever before. The combination of these factors has put considerable pressure on the existing infrastructure, leading to increased demands in inspection and maintenance of rail assets.

This paper studies track deterioration from geometric aspects and its influencing factors with a case study for railway line of pan – European Corridor 10 on the territory of North Macedonia.

The analysis made in the paper will obtain results that would reflect the actual state of the railway infrastructure on the territory of the Republic of North Macedonia..

Keywords: track geometry degradation, maintenance, measuring vehicle, railway quality, railway management, measurement visualization

1. INTRODUCTION

The maintenance of railway infrastructure is an economic issue with high costs. Predicting damage and degradation of railway geometry and planning and organizing maintenance work requires some experience and knowledge of various indicators of railway quality. The decision to maintain and intervene on the route requires a precise and qualitative definition of the goals to be achieved. These goals refer to the quality, quantity, and price of the performed maintenance. Therefore, it is necessary to define the maintenance process following the predefined goals and set good indicators to check the expected performance [1].

In maintaining the railway infrastructure, it is crucial to measure and maintain the geometry of the railway at an acceptable level and to minimize the risk of trains derailing. Therefore, the quality of the route geometry must be assessed to determine the levels of deviation. When the measured variation is above a predetermined limit, travel speeds must be reduced, affecting travel comfort and increasing

transport costs. Thus, the correct geometry of the route can be considered a measure of both safe travel and travel quality [2].

Route degradation is a complex process. The quality of the route is assessed according to the condition of its components and its geometry. The poor state of one part usually contributes to the degradation of the other [3].

The complexity of studying railway degradation comes from the diversity of their components' characteristics and the system's traffic [4].

The trans-European networks and the pan-European corridors are designed to enable traffic connection in several directions to satisfy the needs for the transport of goods and people. Therefore, in the Republic of North Macedonia, it is necessary to develop the railway network to provide a regional connection with neighboring railway networks

and contact with the nearest ports in neighboring countries and meet the principle of competition in the transport sector.

Macedonian railway infrastructure is included in the network of pan-European corridors and routes:

- Corridor 10: Thessaloniki - Skopje - Nis - Belgrade - Zagreb - Ljubljana - Salzburg,
- Corridor 10d: Veles - Prilep - Bakarno Gumno - Bitola - Florina (Florina),
- Corridor 8: Durres - Tirana – Kafasan / / Lin - Kicevo - Skopje - Kriva Palanka - Gjueshevo - Sofia - Plovdiv - Stara Zagora - Varna / Burgas,
- Route 10 - Kosovo - Skopje border.

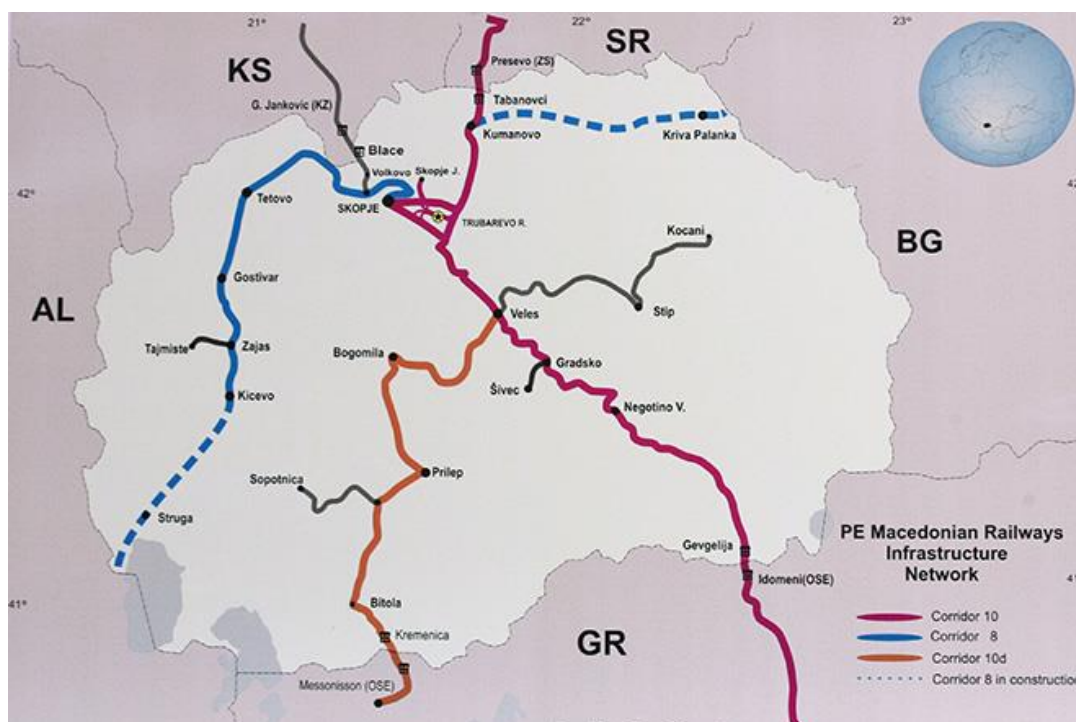


Figure 1. Pan-European Corridors on the territory of North Macedonia

The development of the railway infrastructure in the Republic of Northern Macedonia must be in function of sustainable and balanced development of the country and thus lead to the inclusion of the Republic of Northern Macedonia in the common market of the European Union.

Consequently, it is necessary, above all, on the railways that are important for the international traffic, to improve the railway infrastructure and

harmonize in the technical-technological needs required for the trans-European railways to coordinate the development of the railway infrastructure with the others. Types of transport (road, sea, air, and combined) and most importantly, through modernization, overhaul, and maintenance of the existing railway infrastructure to supplement the necessary infrastructure capacity to increase the volume and functionality of rail transport.

2. RESEARCH SCOPE

The main problem that will be elaborated on in this paper refers to the research of the condition of the tracks of the railway infrastructure on the territory of North Macedonia with a particular reference to the geometric degradation of the track and the analysis of influential parameters that lead to the appearance of degradation of the track.

The research subject is the analysis and measurement of geometric degradation of the railway from Corridor 10 on the territory of North Macedonia.

The corridor is on route Tabanovce - Skopje - Veles - Gradsko - Demir Kapija - Gevgelija - Bogorodica. The railway is intended for mixed traffic (passenger and freight). The main railway line from Corridor 10 that runs along the Republic of Macedonia has a total length of 214.9 km and is electrified along its entire length, modernized, with an average speed of 90 km/h.

3. RAILWAY LINE ON CORRIDOR 10

The railway track on Corridor X is a single track and the present railway line allows a maximum speed of trains between 60 and 80 km/h. This situation is caused principally of geometry of railway line, which has built in XIX century, and in small part of bad condition of superstructure and substructure.

The total length of railway track is 214,9km and total length in the curve line is 114,1km; so the 53% of the railway track is in curve line and 47% in alignment.

The analysis of number and length of curve lines for three main sections on Corridor 10 shows that the section Tabanovci – Skopje has not any curve lines with radius less or equal than 300 m, and the section Skopje – Veles has about 12% of length in curve lines with radius between 250 m and 300 m.

There are 6 tunnels through Corridor 10 and total length of tunnel is 1029,4 m. All tunnels are located on the sections Skopje-Veles and Veles-Gevgelija. The speed of trains is limited to 60 km/h because in tunnel sections the radiuses are less than 350m.

The total number of bridges is 91 with total length of 2312 m. About 52% are steel bridges whose length is 1778 m, or 77% of total bridges length. All bridges on Corridor 10 can support

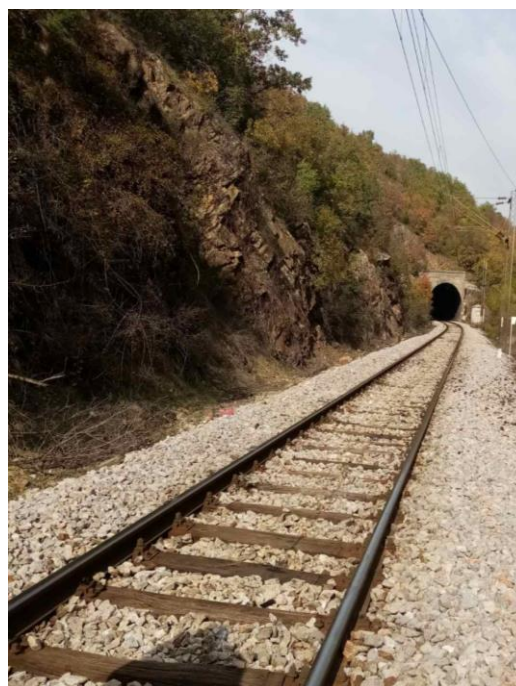


Figure 2. Corridor 10 on section Skopje – Veles
Source: Prospection in situ

axel load of 225 kN/80kN/m and they are classified in D4 – UIC group.

There are also 80 drainage culverts on the section Tabanovce-Skopje (1,6/km), 118 on the section Skopje-Veles (2,3/km), and 298 on the section Veles-Gevgelija (2,6/km).

The total railway track consists of continuous welded rails (CWR). The most used rail is S49 on 97,3% of track length and of 2,7% of rail length have rail type S54 (sections line between stations Tabanovci – Kumanovo and Romanovci – Miladinovci).

The timber is dominant with around 89% of total number of 329 727 sleepers on railway track of Corridor X. The normal sleeper spacing is between 600 - 650 mm.

The most wide - spread fastenings system on the track is rigid K-system for each section where the timber sleepers are set and elastic fastenings SKL-14 with greater elasticity in the case of prestressed concrete sleepers.

The ballast is constituted from crushed limestone with grading of 25/60 mm for sections between railway stations.

The thickness of the ballast bed is estimated 30 to 35 cm measured from the underside of the sleeper. The ballast is contaminated frequently by attrition of the ballast material or upwards penetration of fine particles in the form of a clay mixture or slurry.



Figure 3. Superstructure with railway track of CWR
Source: Prospection in situ

4. TRACK GEOMETRY MEASUREMENTS

Railway management institutions in all European countries are obliged to carry out measurements and technical and diagnostic tests of the elements of the railway infrastructure. These actions aim to determine the objects and devices' actual (real) condition. The information collected in this process is the basis for approving decisions to continue exploitation, take preventive measures, or start repairs. Such measurements require specialized construction tools adapted to the specific nature of the railway environment and to an accuracy that meets the requirements specified in the sector guidelines [5].

Infrastructure operators have recognized this and have changed their attitude towards measuring vehicles, especially in recent years. Gauges are no longer considered just a safety instrument but, in the broadest sense, enable "the right action at the right time." Changes in the meaning of measuring vehicles and new technological possibilities in measuring technology, primarily video surveillance, have led to significant technological advances in recent years [6].

The Track Geometry Measurement System provides accurate and reliable track data for immediate and long-term maintenance planning. The system can be installed on virtually any rail bound vehicle and provides all the data necessary for the optimum management of track assets [7].

For measuring, recording and analysis of the track geometry, the standard equipment of every track recording car is the track geometry

measuring system. This consists of an inertial navigational measuring system with integrated GPS positioning and a dual optical gauge measuring system. Track geometry faults with wavelengths up to 200 m can be recorded, regardless of the measuring speed [8].



Figure 4. Mermec measuring vehicle

The track geometry measurements of the railways on the territory of North Macedonia were carried out by measuring vehicles of the company Mermec (Figure 4) in 2010 and 2013.

The system offers highly accurate measurements with real time reports of exceedances of allowed geometry.

The vehicle measures:

- track gauge - the distance between the inner surfaces of the head rails measured 14 mm lower than the head tops,
- cross level/cant - difference in the height of rail heads in one cross section,
- twist - difference in cant on the base length of 5 m,
- alignment (D1 and D2) - horizontal deviation of the rail head from a base line (10 m long) measured independently for both rails,
- longitudinal level (D1 and D2) - vertical deviation of the rail from a base line made by points of tangency of 2 wheels with the rail (base distance equals to 10 m). It is measured independently for both rails.

According with the European Standard EN 13848-5, the thresholds used for defects detected by Track Geometry Measurement System are reported in the following tables:

Table 1. Thresholds for gauge measurement

Gauge [mm]			
IAL		IL	
Minimum	Maximum	Minimum	Maximum
-11	35	-9	30

Table 2. Thresholds for twist measurement

Twist [%]			
IAL		IL	
Minimum	Maximum	Minimum	Maximum
-7	7	-5	5

Table 3. Thresholds for alignment measurement

Alignment [mm]			
IAL		IL	
Minimum	Maximum	Minimum	Maximum
-17	17	-11	11

Table 4. Thresholds for longitudinal level measurement

Longitudinal level [mm]			
IAL		IL	
Minimum	Maximum	Minimum	Maximum
-26	26	-13	13

5. DATA COLLECTION AND ANALYSIS

One of the purposes of this quantitative analysis is to correlated track geometry data from the measurement campaigns with operating conditions, weather, superstructure elements and maintenance activity history.

Track geometry measurements were performed in 2010 and 2013 using a measuring vehicle from the Italian company Mermec.

The results presented are based on the data collected from two measurements during three years, from 2010 to 2013.

Most of this data must be visualized correctly for users to gain insight into the actual behaviour of the objects in question. Hence the utter need for high-quality visualization when it comes to infrastructure management. This is because, sometimes, even looking at the data, if displayed innovatively and adequately, can help infrastructure managers derive invaluable insights.

The Ramsys software system (Railway Asset Management System) developed by Mermec

interprets the raw data from track geometry measurements on a user-friendly module.

Figure 5 shows some of the visualization capabilities of the Ramsys system. The important thing here is the complete freedom of the user in terms of defining Views and customizing them to his/her own needs and liking, as well as freedom in combining various data types in any user-defined way in order to gain better insight into mutual dependencies between the data, correlations in order to search for the root cause of the problems.

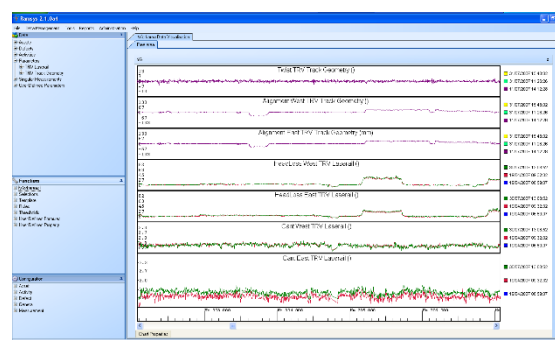


Figure 5. Measurement visualisation in Ramsys system

From the analyses data it is concluded that 22% of the railway network has been reported to be in very good and good condition, where approximately 70%-100% of designed speed can be achieved. The largest part of the railway network is in medium condition, with larger variations in the maximum allowed speed. On these sections, approximately 42%-88% of designed speed can be achieved. 31% of sections have been reported to be in a poor condition, where on average 55% of designed speed can be achieved (Figure 6).

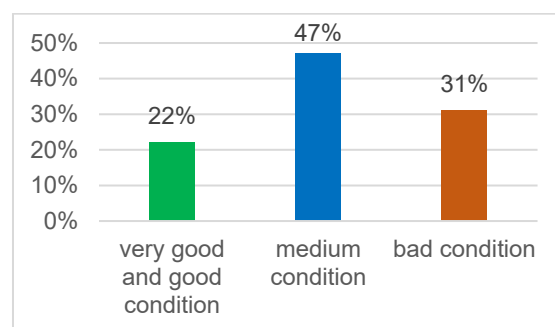


Figure 6. Condition of the railway Corridor 10 on the territory of North Macedonia

At this moment, the railway can respond to the current traffic volume. However, the fact that only 11% of the railway from corridor 10, which passes through the Balkan countries, is classified as a favourable condition, while the

rest has medium or unfavourable conditions, indicates the need for reconstruction.

The primary interventions in the short term should ensure higher speed and technical standards of the network.

6. CONCLUSION

The available documents concluded that there is almost no record of the maintenance and renewal of railway infrastructure elements carried out over several decades. At best, an unsystematic approach to maintenance and renewal is present.

However, the actual and exact level of this poor condition, as well as the locations bearing the worst conditions endangering the safety of traffic, remain vastly unknown. This is due to the utter lack of:

- Consistent information about the exact location of all the Railway Infrastructure Assets,
- Consistent information about the systematic and regular Railway Infrastructure Assets condition measurements, especially over a more extended period,
- Methods, knowledge, and means for large-scale systematic Railway Infrastructure Assets condition-data collection,
- Methodology, standards, and tools for the processing and analysis of the collected condition-data to schedule the appropriate Maintenance and Renewal works.

Improving the condition of the superstructure of the busiest sections of Corridor 10 should be a priority task. The condition of the track on certain sections of the main line is terrible due to the total depreciation of the superstructure elements. This situation today leads to a reduction in train speeds and increased operating costs.

Considering that the price of road transport will largely depend on the oil prices in the world markets, the railways should pay particular attention to using these external factors for a more significant attraction of passengers. It will be of great importance to increase the travel speeds of passenger trains by reconstructing the track from Corridor 10.

For more efficient maintenance, it is necessary to acquire additional machinery that will be needed for more economical and higher-quality operations.

REFERENCES

- [1] Antonio Ramos Andrade, Paulo Fonseca Teixeira, "Uncertainty in Rail – track geometry degradation: Lisbon – Oporto Line Case Study", *Journal of Transportation Engineering*, March 2011
- [2] Genovefa Kefalidou, David Golightly, Sarah Sharples, "Identifying rail asset maintenance processes: a human – centric and sensemaking approach", *Cognition, Technology & Work* (2018) 20:73–92 <https://doi.org/10.1007/s10111-017-0452-0>
- [3] Iman Soleimanmeigouni, Alireza Ahmadi, Arne Nissen, Xun Xiao (2020) "Prediction of railway track geometry defects", *Structure and Infrastructure Engineering*, 16:7, 987-1001, DOI: 10.1080/15732479.2019.1679193
- [4] A.A. Iman Soleimanmeigouni, "Track geometry degradation and maintenance modelling: A review", *Proceedings of the Institution of Mechanical Engineers, Part F: Journal of Rail and Rapid Transit*, 2016
- [5] Dr.-Ing. Dr. techn. Florian Auer, *Multi-function track recording cars*, 2013.
- [6] Zdenka Popovic, Filip Trpceviski, Isidora Pancic, Luka Lazarevic (2014). *Harmonizacija evropskog kvaliteta koloseka, GRADJEVINSKI MATERIJALI I KONSTRUKCIJE* 57 (2014) 1 (29-44)
- [7] Jovanović S, MER MEC S.p.A., Italy (2007): *Modern railway Infrastructure Asset Management, Rail-Tech Russia 2007*, Moscow, Russia, June 18-20, 200723
- [8] Dr.-Ing. Dr. techn. Florian Auer, *Multi-function track recording cars*, 2013.

Hartmut Pasternak

Brandenburg University of Technology,
Institute of Civil and Structural Engineering,
Cottbus, Germany
Hartmut.Pasternak@b-tu.de

Natasa Zivaljevic-Luxor

University of Nis, Faculty of Civil Engineering
and Architecture, Nis, Serbia
nluxor@gmail.com

THE COLOSSUS OF PRORA – BUILDING HISTORY AND NEW BEGINNING

Prora is a beach resort built in the 1930-ies on the island of Rügen, Germany. The structure itself extends impressive 4.5 kilometer. The design won the Grand Prix award at the 1937 Paris World Exposition. Decisive for the Monument Protection Authority were "the impressive and characteristic cubic structure of the building body" and the "reinforced concrete skeleton construction, cast on site". Never finished, it is now built into luxury apartments.

Keywords: large on-site cast reinforced concrete skeleton construction, heritage, intervention strategies techniques

1. INTRODUCTION

Prora is a beach resort on the island of Rügen, in the German part of the Baltic Sea. After smashing the German Unions in 1933, it was planned as a huge holiday resort for growing middle class of industrial workers, and partly built between 1936 and 1939. It is situated 160 metres from the beach and follows the cost line. The structure itself extends impressive 4.5 kilometres (Fig.1), that's why Colossus of Prora and it is listed as heritage since 1992.



Figure 1. View Prora complex [1]

2. ORIGINAL ARCHITECTURAL CONCEPT

The structure, an on-site cast reinforced concrete skeleton construction, consists of eight housing blocks, each 500m long and six storey high, which were intended to accommodate 20,000 guests at once. Each room was directed to the East, overlooking the sea. That's why the depth of the housing blocks was 10,5 meters on the ground floor and on the second floor and only 8 meters above. The ground floor was planned/designed to be used by children's homes, shops and staff apartments.

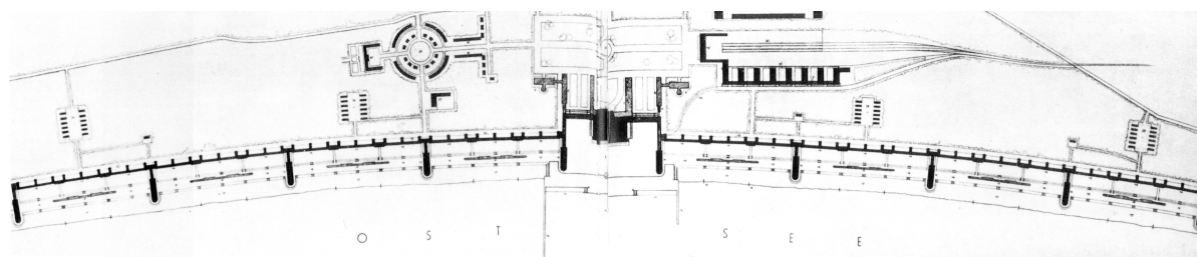


Figure 2. Original ground plan [2]

The "Community Housing", a 110 m tower, is positioned perpendicularly to the frontline of the housing blocks, ahead of them, in the beach area. It is 3.5 storey high structure. In its basement, there were utility rooms and dining rooms, while on the second floor, there were cafeterias and restaurants with terraces; in a mezzanine, the area was reserved for writing, reading and children playrooms, and on the upper floor, for bowling and billiard. On the backside of the building there were lifts at a distance from 50 m.

All housing blocks (Fig. 2) were designed by Cologne architect Clemens Klotz (1886–1969). The main hall for festivities (Fig. 3, in the upper right corner) was designed by Erich zu Putlitz (1892-1945), an architect from Hamburg. The design won the Grand Prix award at the 1937 Paris World Exposition, attracting lot of attention by its size.

The main hall for festivities (Fig. 3, in the upper right corner) was designed by Erich zu Putlitz (1892-1945), an architect from Hamburg. The design won the Grand Prix award at the 1937 Paris World Exposition.

Klotz designed mostly for Cologne and surroundings, and he accepted several non-military project requests from National-Socialist Party. In the very beginning of 20th century, Klotz was a member of Deutscher Werkbund, which later led to foundation of Bauhaus. He was engaged in planning Cologne, and he designed Munich train station, which reveals his interest in huge structures, which reshape the landscape. Klotz caught the spirit of the epoch by choosing cast concrete as structural element. The façade was simple, with few details. Apart from it, it has little resemblance with other grandiose architectural designs from the same period, for example done by Le Corbusier. Colossus is firmly on the ground, not leaving ground level free for communication, as one might expect. The proportions are determined by simplified function, and it is extreme and intentionally not balanced.

The uniformity of the architecture reveals that functionality in architecture was very important

and that concept had strong political background (KdF - Kraft durch Freude = Strength Through Joy).



Figure 3. Planned design [3]

3. ORIGINAL BUILDING DESIGN AND CONSTRUCTION

The structure of the housing blocks is an on-site cast reinforced concrete skeleton construction (Fig. 4).



Figure 4. Skeleton construction

The grid was 5 m x 5 m. The load-bearing exterior walls are made of masonry, while the window lintels consist of reinforced concrete. The cast concrete technology was already widely known and accepted at that time. Reinforced strip and individual foundations (C20/25) have been carried out. The thin ceiling of the housing blocks consists of reinforced concrete (C20/25) with steel bars ($d=6\text{mm}$ and $a=5\text{cm}$). Fig. 5 shows a cut-out roofing.



Figure 5. Removed roofing



Figure 6. Building under construction [2]

All major construction companies of the Third Reich with nearly 9,000 workers were involved in this project (Fig. 6). Some of the companies which were engaged, e.g. Dyckerhoff & Widmann, Hochtief, Polensky & Zöllner, exist to this day. The building site was stopped by World War II. The original design (Fig.2) included swimming pools, a cinema and a theatre, which were not built at the time.

Each guest room was of 4.75 x 2.25 metres in size, had two beds, a wardrobe, a seating corner and a sink, all designed according to the modular principle. Figure 7 shows the outlook of typical room. The guest blocks included communal toilets, showers and bathrooms on each floor.



Figure 7. Single room (photo: Th. Schramm [4])

4. COLOSSUS AS HERITAGE

The Colossus of Prora is interesting from two sides – as an extraordinary huge structure, and as an example of pre-WW II architecture which reflects values of the epoch. Basically, they are values of a former totalitarian regime, but superposed to values of architecturally advanced society, which also gave Bauhaus to the World, among other contributions, in years immediately before the Colossus was erected.

The complex was listed as heritage in 1992, because it was considered to be rare example of the Third Reich Architecture, built for entertainment and recreation, and not either for industrial or military purpose. Decisive for the Monument Protection Authority were: "the impressive and characteristic cubic structure of the building body", the "reinforced concrete skeleton construction, cast on site" (Fig. 8), and, in addition, that it should not be left as "abandoned building".



Figure 8. Interior under reconstruction

Five of the 8 blocks still exist. The last among many attempts for revitalisation of Colossus came in 2012, when the complex was sold to private investors, whose plan for rehabilitation included luxury holiday apartments and a 5-star hotel, for 3000 people, with an indoor swimming

pool and a wellness area (which were partially realized). By removing interior walls, it became possible to receive larger apartments (Fig.9).

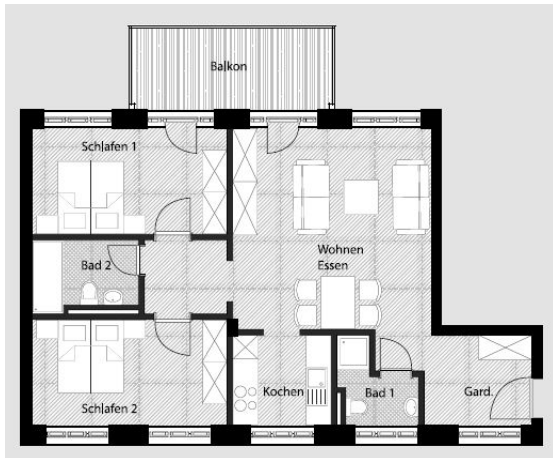


Figure 9. Floor plan of a 3-room apartment and living room [5]



Figure 10. Façade

Additional measures were: reinforcing the foundations, cutting out the masonry walls for doors and dismantling the inner concrete walls. One of the requirements of Monument Protection Authority was to keep the board formwork of the ceilings visible. On the other hand, they agreed to equip every apartment by a terrace or light cantilevered balcony (Fig.10). Freestanding parking houses have been built.



Figure 11. Escape stairs

Colossus reflects genuine sensibility of its architect, Klotz, which has not changed much even in decades of architecture practice following the end of War. Klotz's understanding of architecture, served the particular political regime, but it reflects values which are praised, in general, by every totalitarian regime. Therefore, part of Colossus is justly preserved as museum. The rest of it significantly changed. It was widely accepted that Colossus must be adopted for new purpose, with interventions including façade remodeling (Fig 10). In addition, escape stairs were installed for fire protection (Fig.11).

5. DISCUSSION AND CONCLUSION

Embracing principles of sustainability, in nowadays Europe, it is common to preserve outdated, abandoned industrial buildings without particular artistic values, aesthetically insignificant, for the sake of their size (being hard to demolish), its symbolic value or/and as

element of cultural landscape. It is unusual to apply such approach on a holiday resort, but in general, that is what happened in this case. Colossus is preserved for its size, which defines a skyline integrated with beach of the Baltic Sea. Regardless of its beauty, according to nowadays criteria, the Colossus generated cultural landscape, and became landmark whose loss would make the area unrecognisable. Colossus was different from other war buildings, because it is not preserved for sake of some 'threatening memory', normally based on aesthetic of ugliness (as in case of concentration camps), and therefore its rarity, as much as the size, make it valuable and worthy of preservation.

The logic of its revitalisation is essentially the one typically applied to industrial buildings – with loose limits to intervention, allowing changes of façades. Economic sustainability is expected to be provided on site (which is not typical). It has little economic impact to the development of the area. – which is at the moment considered to have already too many tourists. From the point of view of concept of economical sustainability, Colossus revitalisation can be compared with very successful City G in Vienna (Gas factory revitalisation in Siemering), and probably learn from it. Similar to City G, most of the Colossus will turn into comfortable apartments for residents, and the rest of it in variety of carefully chosen purposes.

The environmental sustainability of Colossus revitalization is somewhat ambiguous. Such building cannot be good for the environment, generally speaking. However, it exists very long and living environment is well adjusted to it by now, therefore radical change would be shocking. Demolishing such huge building, as alternative to preservation, would produce huge amount of debris which would be devastating for the environment. So, from point of view of sustainability, preservation is fully justified.

Finally, Colossus remains mostly challenging from the point of view of heritage management. It is well known that it is possible to adapt even an extremely huge, over 80-year-old, building complex for needs of contemporary life. However, it is not yet proven that current strategy would be entirely successful and turn Colossus in Prora into Colossus of Prora.

REFERENCES

- [1] https://www.google.de/search?q=der+aufbau+prora&source=inms&tbm=isch&sa=X&ved=0ahUKEwi718jY6fjSAhVFiwKHetTDPkQ_AUIBigB&biw=1259&bih=664&dpr=1#imgrc=wZgyzd a6DdwpMM:
- [2] Dokumentationszentrum Prora, <http://www.proradok.de/en/photo-gallery/>
- [3] <http://www.ndr.de/kultur/geschichte/schauplaetze/Der-Koloss-von-Ruegen,prora113.html>.
- [4] https://de.wikipedia.org/wiki/Datei:Prora_zimmer.jpg
- [5] Prora Solitaire Hotelbroschüre 2017.pdf